

# Reconnection-controlled decay of magnetohydrodynamic turbulence and the role of invariants

David N. Hosking<sup>1,2,\*</sup> and Alexander A. Schekochihin<sup>2,3</sup>

<sup>1</sup>*Oxford Astrophysics, Denys Wilkinson Building, Keble Road, Oxford OX1 3RH, UK*

<sup>2</sup>*Merton College, Merton Street, Oxford, OX1 4JD, UK*

<sup>3</sup>*The Rudolf Peierls Centre for Theoretical Physics, University of Oxford, Clarendon Laboratory, Parks Road, Oxford, OX1 3PU, UK*

(Dated: July 3, 2022)

We present a new theoretical picture of magnetically dominated, decaying turbulence in the absence of a mean magnetic field. With direct numerical simulations, we demonstrate that such turbulence is governed by the reconnection of magnetic structures, and not by ideal dynamics, as has previously been assumed. We obtain predictions for the magnetic-energy decay laws by proposing that turbulence decays on reconnection timescales, while respecting the conservation of certain integral invariants representing topological constraints satisfied by the reconnecting magnetic field. As is well known, the magnetic helicity is such an invariant for initially helical field configurations, but does not constrain non-helical decay, where the volume-averaged magnetic-helicity density vanishes. For such a decay, we propose a new integral invariant, analogous to the Loitsyansky and Saffman invariants of hydrodynamic turbulence, that expresses the conservation of the random (scaling as volume<sup>1/2</sup>) magnetic helicity contained in any sufficiently large volume. We verify that this invariant is indeed well-conserved in our numerical simulations. Our treatment leads to novel predictions for the magnetic-energy decay laws: in particular, while we expect the canonical  $t^{-2/3}$  power law for helical turbulence when reconnection is fast (i.e., plasmoid-dominated or stochastic), we find a shallower  $t^{-4/7}$  decay in the slow ‘Sweet-Parker’ reconnection regime, in better agreement with existing numerical simulations. For non-helical fields, for which there currently exists no definitive theory, we predict power laws of  $t^{-10/9}$  and  $t^{-20/17}$  in the fast- and slow-reconnection regimes, respectively. We formulate a general principle of decay of turbulent systems subject to conservation of Saffman-like invariants, and propose how it may be applied to MHD turbulence with a strong mean magnetic field and to isotropic MHD turbulence with initial equipartition between the magnetic and kinetic energies.

## I. INTRODUCTION

The nature of the decay of magnetohydrodynamic (MHD) turbulence is an important outstanding problem in fluid dynamics, with far-reaching consequences in astrophysics, from the evolution of primordial magnetic fields in cosmology [1] to the dynamics of the solar wind [2]. Naturally, the subject of decaying turbulence is one with a long history. In the hydrodynamic case, the basic problem of determining the exponent of the energy-decay power law was solved by Kolmogorov, in the third of his seminal 1941 papers on turbulence [3]. Kolmogorov’s approach can be summarised as follows: (i) identify an ideal invariant that is better conserved than the kinetic energy, then (ii) posit a decay of the kinetic energy, occurring on the dynamical timescale, that conserves that invariant. In the case of hydrodynamic turbulence, Kolmogorov identified the Loitsyansky integral,

$$I_L = - \lim_{V \rightarrow \infty} \int_V d^3\mathbf{r} r^2 \langle \mathbf{u}(\mathbf{x}) \cdot \mathbf{u}(\mathbf{x} + \mathbf{r}) \rangle, \quad (1)$$

as the relevant invariant. Physically, the conservation of  $I_L$  represents the net conservation of angular momentum of the turbulent eddies [4, 5]. Note, though, that the

invariant controlling the decay is not simply the mean angular momentum,  $\langle \mathbf{L} \rangle = \langle \mathbf{r} \times \mathbf{u} \rangle$ , which, while conserved, is zero by isotropy. The Loitsyansky integral is therefore an example of an invariant that encodes the conservation of a quantity that individual eddies are expected to possess, but that has vanishing mean value due to its randomly directed nature.

Eq. (1) implies the scaling  $U^2 L^5 \sim \text{const}$ , where  $L$  is the correlation scale of the turbulence, and  $U$  is the typical velocity at that scale. Together with the identification of the dynamical timescale as  $\tau \sim L/U$ , this is enough to fix the decay rate of the kinetic energy  $E = U^2/2$ , as

$$\frac{dE}{dt} \sim -\frac{E}{\tau} \sim -\frac{E^{3/2}}{L} \sim -E^{17/10}, \quad (2)$$

which results in Kolmogorov’s famous decay law

$$E \sim t^{-10/7}. \quad (3)$$

This result has been confirmed to excellent precision numerically [5, 6].

In this paper, we show how Kolmogorov’s philosophy can be adapted to MHD turbulence. Historically, two problems have hindered such attempts. First, there appear to exist two fundamentally different regimes. For helical field configurations, where the volume-averaged magnetic-helicity density,  $\langle h \rangle = \langle \mathbf{A} \cdot \mathbf{B} \rangle$ , is non-zero,  $\langle h \rangle$  provides a scaling that can be used to constrain the decay,

\* david.hosking@physics.ox.ac.uk

$B^2L \sim \text{const}$ , where  $B$  is the typical size of the magnetic field at the correlation scale  $L$ . However, magnetic helicity is not sign-definite, so there also exist non-helical field configurations, for which  $\langle h \rangle \ll B^2L$ . For such fields, the conservation of  $\langle h \rangle$  does not impose a constraint on the decay. In this work, we show that even in such cases, the decay is still controlled by helicity conservation, in a manner analogous to the control of the decay of hydrodynamic turbulence by angular-momentum conservation.

Second, since, besides velocity, MHD has an additional field,  $\mathbf{B}$ , there is no longer a dimensional inevitability in the identification of the decay timescale, as there was in hydrodynamics. Previous treatments [7–10] have assumed the Alfvénic scaling  $U \sim B$  in order to determine the ideal timescale uniquely, though this is not well reproduced in numerics, where  $B \gg U$  appears to be maintained if it was true initially, and, furthermore, for helical magnetic fields, a faster decay of the kinetic energy than the magnetic energy is often observed [1, 9, 11–15]. In fact, it is intuitively clear that relaxation on ideal timescales may not be possible for a strong initial magnetic field, because of the topological constraints imposed by magnetic-flux freezing. For non-trivial initial magnetic topologies, relaxation can only occur on the timescale on which these topological constraints may be broken, i.e., the magnetic-reconnection timescale. The resulting evolution would consist of coalescences of neighbouring magnetic structures, provided they are sufficiently localised, which leads to a natural explanation for the inverse transfer of magnetic energy observed in both helical and non-helical decaying MHD turbulence [11, 16–22]. Such a reconnection-controlled decay has been shown to occur in two-dimensional decaying turbulence [23], and numerical evidence in its favour has been presented for three-dimensional, non-helical turbulence too [22], though with an essentially two-dimensional interpretation that is not the one that we shall propose below.

Unless the values of the dissipation coefficients are sufficiently small for reconnection to occur in the plasmoid-dominated [24] or stochastic [25] regime (currently numerically inaccessible, due to the resolution requirements imposed by the need for a sufficiently small-scale initial condition), the evolution should occur in the ‘Sweet-Parker’ reconnection regime [26, 27]. Sweet-Parker reconnection is defined by the conditions of (i) efficient conversion of magnetic energy to kinetic energy of reconnection outflows, and (ii) a balance between the inductive term,  $\nabla \times (\mathbf{u} \times \mathbf{B})$ , and the resistive dissipation term in the MHD induction equation, so that reconnection occurs in a time-invariant manner. This last requirement means that reconnection-controlled decaying turbulence in the Sweet-Parker regime is very different from decaying hydrodynamic turbulence, in that it is sensitive to the precise form of the dissipation term. Importantly, this means that different decay power laws are expected in numerical simulations depending on whether Laplacian dissipation,  $\propto \eta_2 \nabla^2 \mathbf{B}$ , or hyper-dissipation,  $\propto \eta_n \nabla^n \mathbf{B}$ ,

is employed. This fact has not been widely appreciated, and leads to a simple test of whether reconnection indeed governs the decay: simulations at moderately large (but not so large so as to be in the ‘fast’ reconnection regime) Lundquist numbers should exhibit different power laws for decay depending on the order of hyper-dissipation,  $n$ . In this paper, we present such simulations, conducted with the incompressible, spectral MHD code Snoopy [28]. They turn out to be in excellent agreement with these expectations. We describe our numerical setup in Appendix C.

An outline of the rest of this paper is as follows. In Section II, we consider the decay of helical MHD turbulence from a magnetically dominated state. Since magnetic helicity is better conserved than magnetic energy in the limit of vanishing resistivity, helicity is precisely a quantity that can control the evolution in the same way as the Loitsyansky integral does in hydrodynamics. Applying a Kolmogorov-style argument to helicity conservation for a decay occurring on the ideal timescale,  $L/B$ , yields a power law of  $t^{-2/3}$  for both the magnetic and kinetic energies [7, 9, 10], though this decay law is not well-supported by numerics, where a shallower decay law for magnetic energy, and a steeper decay law for kinetic energy are typically observed [1, 9, 11–15, 29]. We show that both of these results are expected for a decay occurring via magnetic reconnection in the Sweet-Parker regime. In particular, we show that the magnetic energy should decay as  $t^{-4/7}$  if reconnection occurs in the Sweet-Parker regime, with  $t^{-2/3}$  only achieved by fast reconnection. We find that the faster decay of kinetic energy is a natural consequence of the changing aspect ratio of the Sweet-Parker sheets to which the dominant fluid flows are confined.

In Section III, we consider the decay of non-helical MHD turbulence from a magnetically dominated state. The mechanism controlling this type of decay has so far remained unknown: because the mean helicity density vanishes, its conservation cannot be used to derive a scaling relation relating  $B$ , the characteristic magnetic field, to its characteristic length scale  $L$ . Numerically, decay laws for both the magnetic and kinetic energies of close to  $t^{-1}$  have been observed [15, 18–20, 22], though there is no definitive theoretical explanation for this behaviour. An influential idea is that in the absence of an integral invariant, the decay might satisfy the well-known scaling symmetry of the MHD equations [30], including dissipative terms. Such a decay would have a  $t^{-1}$  power law [31]. Another suggestion is that the non-helical decay is effectively two-dimensional. In this case, it is the conservation of ‘anastrophy’, or the square of the magnetic vector potential, that should control the decay. A Kolmogorov-style argument then leads to a  $t^{-1}$  power law whether the decay occurs on the ideal [15, 19], or the Sweet-Parker [22] timescale (see Appendix A). That both treatments predict the same power law is a coincidence related to the fact that anastrophy conservation implies constant Lundquist number for  $n = 2$  resistive dissipation [23] (in-

identally, the scaling argument is essentially this same point with the direction of implication reversed). However, it is not clear why fully three-dimensional, isotropic turbulence should two-dimensionalise in this way, nor why any special significance should be given to constant Lundquist number. Indeed, we show in Section III that both are inconsistent with numerical evidence.

Instead, we propose a treatment of the non-helical decay controlled by the conservation of fluctuations in magnetic helicity. The key point is that the vanishing of the total magnetic helicity does not necessarily imply that any given magnetic field structure is non-helical. Indeed, non-helical magnetic structures generally relax on ideal timescales to zero magnetic energy, assuming they are not constrained by higher-order topological invariants. We therefore expect that the natural state of the turbulence will be to contain a collection of helical structures, though there will be equal abundances of positive- and negative-helicity structures so that the zero-overall-helicity constraint is satisfied. For such a turbulence, we identify a new integral invariant whose relation to magnetic helicity is precisely analogous to that of the Loitsyansky integral to angular momentum. We refer to this invariant as the ‘Saffman helicity invariant’, due to the close analogy between it and the integral invariant proposed by Saffman for hydrodynamic turbulence [32], and also between our arguments and the arguments usually associated with the Saffman invariant and its various anisotropic generalisations [5, 33]. As we will show, the conservation of our new invariant implies the scaling  $B^{4/5}L \sim \text{const.}$  This scaling implies a magnetic-energy decay power law of  $t^{-20/17}$  in the Sweet-Parker regime, or  $t^{-10/9}$  in the fast reconnection regime. These power laws are different from  $t^{-1}$ , but are still in excellent agreement with published numerical results, and with our own numerical results presented below. We also find that, for non-helical magnetic fields, the rate at which the aspect ratio of the current sheets changes is much smaller than in the helical case, explaining why a faster decay of kinetic energy is not observed for a non-helical decay.

Finally, in Section IV, we discuss the behaviour of systems with fractional helicity, which we show will ultimately always transition to the fully helical regime as long as the system size is sufficiently large. We also discuss possible applications of the Saffman formalism to wider classes of turbulent decays. As an example, we suggest the existence of a Saffman-type cross-helicity invariant that may control the critically balanced decay of MHD turbulence in the presence of a mean magnetic field, recently studied in [34]. We also conjecture that the simultaneous conservation of both the Saffman-type cross-helicity invariant and the magnetic helicity might govern the initial period of decay of an MHD state starting with  $U \sim B$ .

## II. DECAY OF HELICAL TURBULENCE

We first consider the decay of MHD turbulence from an initial state where magnetic energy dominates kinetic ( $B \gg U$ ), and the magnetic field is helical, i.e., the volume-averaged magnetic-helicity density,

$$\langle h \rangle = \lim_{V \rightarrow \infty} \frac{1}{V} H_V = \lim_{V \rightarrow \infty} \frac{1}{V} \int_V d^3\mathbf{r} \mathbf{A} \cdot \mathbf{B}, \quad (4)$$

is large,  $\sim B^2L$ . The case of initial parity between the two energies ( $U \sim B$ ) will be discussed in Section IV E. Magnetic helicity is a topological invariant – the total magnetic helicity of a collection of flux tubes is equal to the amount of (signed) flux linked by these tubes. As such, its conservation is related to Alfvén’s theorem, which states that for  $\eta_n = 0$ , the magnetic field is frozen into fluid motions, ensuring that all topological invariants are precisely conserved. The special significance of magnetic helicity is that, unlike other topological invariants, it remains approximately conserved (i.e., better conserved than energy) for small but non-vanishing  $\eta_n$  [35]. This statement is true independently of the reconnection regime. A proof, adapted from [36], is as follows.

### A. Helicity is conserved by (hyper-resistive) reconnection

In hyper-dissipative MHD, the evolution of the magnetic helicity in a closed volume whose surface is everywhere normal to  $\mathbf{B}$  satisfies

$$\left| \frac{dH}{dt} \right| = 2\eta_n \left| \int d^3\mathbf{r} (\nabla^n \mathbf{A}) \cdot \mathbf{B} \right|. \quad (5)$$

Note that setting  $n = 2$  here yields the familiar expression in terms of the current helicity. Applying the Cauchy-Schwarz inequality to the integral on the right-hand side, one obtains

$$\left| \frac{dH}{dt} \right|^2 \leq 4 \left| \frac{dE_M}{dt} \right| \eta_n \int d^3\mathbf{r} \mathbf{A} \cdot (\nabla^n \mathbf{A}), \quad (6)$$

where  $dE_M/dt = \eta_n \int d^3\mathbf{r} \mathbf{B} \cdot (\nabla^n \mathbf{B})$  is the rate of magnetic-energy decay due to Ohmic heating. For  $n = 2$ , the other integral in Eq. (6) is just twice the magnetic energy [36]. More generally, we can write

$$\begin{aligned} \eta_n \left| \int d^3\mathbf{r} \mathbf{A} \cdot (\nabla^n \mathbf{A}) \right| &= \eta_n \left| \int d^3\mathbf{r} \mathbf{B} \cdot (\nabla^{n-2} \mathbf{B}) \right| \\ &\sim \frac{dE_M}{dt} \delta_\eta^2, \end{aligned} \quad (7)$$

where  $\delta_\eta$  is the resistive dissipation scale. Eq. (6) then implies

$$\frac{d \log H}{dt} \sim \frac{\delta_\eta}{L} \frac{d \log E_M}{dt}. \quad (8)$$

Eq. (8) states that the rate of change of magnetic helicity is smaller than the rate of the energy decay due to Ohmic heating (which will be even smaller than the true magnetic-energy-decay rate, because magnetic energy can also be converted to the kinetic energy of reconnection outflows) by a factor equal to the ratio of the integral scale to the resistive dissipation length scale, which becomes arbitrarily small as  $\eta_n \rightarrow 0^+$ . *Q.E.D.*

It may appear counter-intuitive that reconnection, a process that, by definition, changes the topology of magnetic field lines, can conserve helicity, a topological invariant. The resolution of this apparent paradox is that self-linkages, i.e., twists of the magnetic flux tube are also associated with helicity. For example, during the unlinking of two linked tori by reconnection to form a single torus, the resulting torus ends up twisted, and the total helicity of the configuration is conserved [35].

### B. Theory of helical decay

The conservation of the volume-averaged magnetic helicity, Eq. (4), implies the scaling

$$B^2 L \sim \text{const.} \quad (9)$$

The remaining ingredient required to compute the magnetic-energy decay law is the decay timescale, as a function of  $U$ ,  $B$  and  $L$ . The simplest possible treatment is to assume Alfvénic dynamics, with  $U \sim B$ , similarity between the integral scales of the magnetic and kinetic energies,  $L$ , and, therefore, a decay timescale  $L/B \sim L/U$ . For future reference, we compute the expected decay power law under such an assumption for a scaling more general than Eq. (9), *viz.*,

$$B^\alpha L \sim \text{const.} \quad (10)$$

Eq. (2) becomes

$$\frac{d}{dt} \frac{1}{2} B^2 \sim -\frac{B^3}{L} \propto -B^{3+\alpha}, \quad (11)$$

with solution

$$B^2 \sim t^{-2/(1+\alpha)}. \quad (12)$$

Now setting  $\alpha = 2$  for helicity conservation, the canonical  $t^{-2/3}$  power law is recovered [7]. However, this prediction has proved to be in poor agreement with numerics, which have found a decay of the magnetic energy closer to  $t^{-1/2}$ , and, unexpectedly, a decay of the kinetic energy faster than  $t^{-2/3}$  [1, 9, 11–15, 29].

These discrepancies are readily resolved by assuming the decay to occur on the reconnection, rather than ideal, timescale. Naturally, the reconnection timescale depends on the reconnection regime, i.e., on whether the reconnection is slow (Sweet-Parker) or fast (plasmoid-dominated [24] or stochastic [25]). Fast reconnection, by definition, occurs on dynamical timescales, so will again produce a

$t^{-2/3}$  decay. However, extant numerical simulations of decaying MHD turbulence mostly probe the slow regime, owing to the large Lundquist numbers and hence large resolutions required for fast reconnection to take place. In this case, the reconnection timescale is

$$\tau_{\text{rec}} \sim S_n^{1/n} \frac{L}{B}, \quad (13)$$

where  $S_n = BL^{n-1}/\eta_n$  is the hyper-Lundquist number. Using Eq. (13) for the decay timescale, Eq. (11) becomes

$$\frac{d}{dt} \frac{1}{2} B^2 \sim -\frac{B^3}{L} B^{-1/n} L^{(1-n)/n} \propto -B^{(2\alpha n + 3n - \alpha - 1)/n}, \quad (14)$$

the solution of which is

$$B^2 \sim t^{-2n/(2\alpha n + n - \alpha - 1)}. \quad (15)$$

Again, for a helicity-conserving decay, we set  $\alpha = 2$  to obtain a power law of

$$B^2 \sim t^{-2n/(5n-3)}. \quad (16)$$

For  $n = 2$  (Laplacian dissipation), the power law is

$$E_M \sim t^{-p_M}, \quad p_M = \frac{4}{7} \simeq 0.57, \quad (17)$$

which is indeed shallower than  $p_M = 2/3$ . Indeed, some recent studies at large resolution have reported  $p_M \simeq 0.58$ , in remarkable agreement with this prediction [15, 29]. However, we caution against direct comparison with those simulations, because they employed time-dependent dissipation coefficients. For numerical studies using  $n = 4$  hyper-dissipation [9], Eq. (15) predicts an even slower magnetic-energy-decay exponent of  $p_M = 8/17 \simeq 0.47$ . This is in excellent agreement with the  $p_M \simeq 0.5$  they found numerically.

It may appear counter-intuitive that reconnection can result in a faster decay of kinetic energy than magnetic energy, as reconnection outflows are typically Alfvénic, i.e., the outflow velocity is approximately equal to the upstream Alfvén speed of the magnetic field prior to reconnection – a condition that is hard-wired into the Sweet-Parker scalings. However, the current sheets, where reconnection occurs, are not volume-filling. Denoting the current sheet width by  $\delta$ , the volume occupied by the current sheet formed when two structures of volume  $L^3$  reconnect and merge is  $L^2\delta$ . Therefore, we expect

$$E_K \sim \frac{\delta}{L} E_M \quad (18)$$

for Alfvénic outflows, where  $E_K$  and  $E_M$  should be understood as the total kinetic and magnetic energies in the system, respectively. This result allows for the possibility of different decay rates for the kinetic and magnetic energy, because the ratio  $\delta/L$  need not be constant in time. For example, with hyper-dissipative Sweet-Parker sheets,  $\delta/L \sim S_n^{-1/n} \sim (BL^{n-1})^{-1/n}$ . For  $B^2 L \sim \text{const}$

[Eq. (9)], we find  $\delta/L \sim E_M^{1-3/2n}$ , which, via Eq. (18), translates to

$$E_K \sim E_M^{2-3/2n}. \quad (19)$$

Thus, kinetic energy is indeed expected to decay more quickly than magnetic energy, simply due to the changing aspect ratio of the Sweet-Parker sheets. For  $n = 2$ , this effect is relatively modest: the kinetic-energy decay exponent is  $5/4$  times greater than the magnetic one, so the decay exponents for  $E_M$  and  $E_K$  are  $p_M = 4/7 \simeq 0.57$  and  $p_K = 5/7 \simeq 0.71$ , respectively. For  $n = 4$ , though, the kinetic-energy decay exponent is  $13/8$  times greater than the magnetic one, so these decay exponents become  $p_M = 8/17 \simeq 0.47$  and  $p_K = 13/17 \simeq 0.76$ .

### C. Numerical results

In simulations with  $n = 2$  dissipation, resolution constraints prevent the use of Lundquist numbers that are sufficiently large to achieve good conservation of the magnetic helicity. Nonetheless, supposing that helicity decays as  $H(t) \sim t^{-p_H t}$ , while  $E_M(t) \sim t^{-p_M t}$ , we expect  $B^{2(1-p_H/p_M)}L \sim \text{const}$ . For small but non-vanishing  $\eta_n$ , therefore, we expect to find an  $\alpha$  somewhat smaller than 2 such that  $B^\alpha L \sim \text{const}$ . We can determine this value of  $\alpha$  numerically by measuring  $E_M(t)$  and

$$L = \frac{2\pi}{E_M} \int dk \frac{\mathcal{E}_M(k)}{k}, \quad (20)$$

where  $\mathcal{E}_M(k)$  is the spectral magnetic-energy density.

As long as  $\eta_n$  is not too large, the decay should still occur on the Sweet-Parker timescale. We can then use Eq. (15) to determine the expected magnetic-energy decay law based on the empirically determined value of  $\alpha$ , and compare with the value measured in our simulations. While we do not expect that this procedure should yield exact agreement between the predicted and empirical decay exponents, as it neglects the role of Ohmic diffusion (which, when  $S_n$  is small, will ultimately become more important to the decay than reconnection), we expect approximate agreement that becomes better as  $S_n$  increases, with  $\alpha$ , therefore, becoming closer to 2.

In Fig. 1, we present the results of such a comparison for  $n = 2$  and  $n = 4$ . This figure shows remarkable agreement between our simulations and the Sweet-Parker decay curves (coloured), despite the fact that we do not reach the asymptotic value of  $\alpha = 2$  with  $n = 2$  dissipation. For  $n = 4$ , we also find excellent agreement, and do reach  $\alpha = 2$ . As other authors have noted [9], the asymptotic scaling is reached much more rapidly in the hyper-dissipative case, and indeed we were forced to choose relatively small values of  $S_n^{1/n}$  in order to populate the part of Fig. 1 with  $\alpha < 2$ . To illustrate this point further, we plot two simulations with  $n = 6$  hyper-dissipation, which also exhibit the  $\alpha = 2$  scaling (and are almost coincident in Fig. 1). The faster attainment

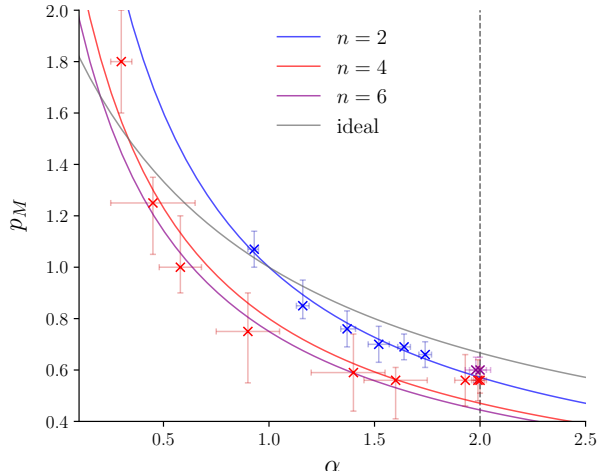


FIG. 1. Relation between the empirically obtained magnetic-energy-decay power-law exponent,  $p_M$ , and the value of  $\alpha$  for which  $B^\alpha L \sim \text{const}$ . Solid curves show the expected relationship, Eq. (15), for decays occurring on the Sweet-Parker timescale, with  $n = 2$ ,  $n = 4$  and  $n = 6$  shown in blue, red, and magenta, respectively. The grey solid curve depicts the ‘ideal’ scaling given by (12). Simulation results are in excellent agreement with the coloured curves, and not with the grey curve. This confirms that the decay takes place on the Sweet-Parker, rather than ideal, timescale. The full set of decay curves from which this plot was derived can be found in Appendix C.

of the correct asymptotic scaling with hyper-dissipation will be important in establishing the correct value of  $\alpha$  for non-helical turbulence, previously unknown, in the next section.

Interestingly, we note that for  $\alpha \simeq 2$ , the decay exponent  $p_M$  is consistently somewhat larger than our theoretical prediction based on Sweet-Parker reconnection. This suggests these simulations may be at the start of the transition to the fast-reconnection regime. We do not find the same transition in two-dimensional simulations (see Appendix A), despite employing even larger Lundquist numbers, which is consistent with the intuitive expectation that fast reconnection should ‘turn on’ more quickly in three dimensions, due to turbulence in the reconnection region.

For the decay of the kinetic energy also, we find that the predictions of the previous section are in good agreement with our simulations, as shown in Fig. 2. The upper panel shows the evolution of the magnetic- and kinetic-energy spectra for a run with  $n = 4$ ,  $\eta_4 = 2 \times 10^{-8}$ , confirming that at any given time, kinetic energy is contained at much smaller scales than the magnetic energy, consistent with the expectation that reconnection outflows should have a width  $\delta \ll L$ . The inset shows the relative sizes of the total magnetic and kinetic energies in the same run, which are in excellent agreement with

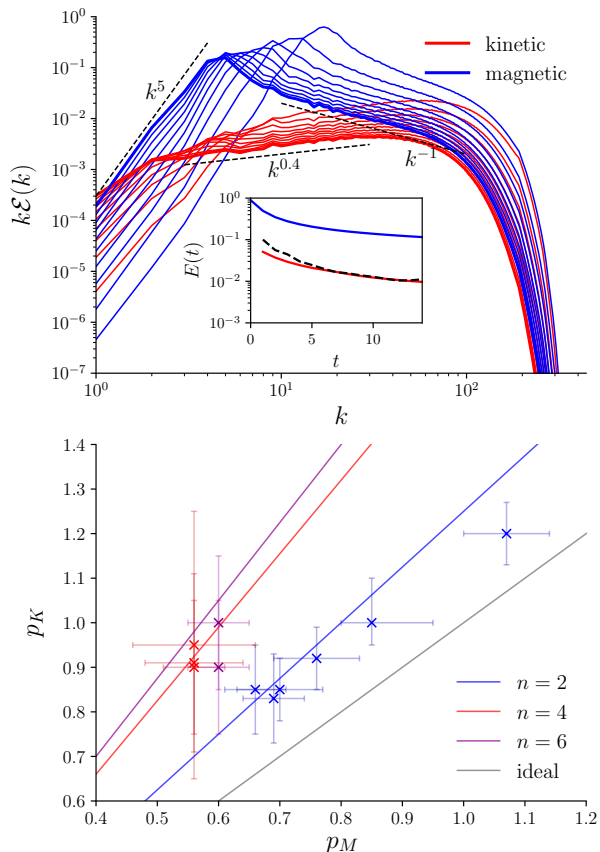


FIG. 2. Top panel: Evolution of  $k\mathcal{E}(k)$ , where  $\mathcal{E}(k)$  is the spectral energy density, for the magnetic (blue) and kinetic (red) energies. These plots are obtained from a helical simulation with  $n = 4$ ,  $\eta_4 = 2 \times 10^{-8}$ . Each plot of  $k\mathcal{E}(k)$  is separated by a time interval of 1.0 between  $t = 1.0$  to  $t = 10.0$  ( $t = 10.0$  in bold), where time is in code units based on normalising the box size and initial mean-square magnetic field to  $2\pi$  and 1, respectively, so that 1 time unit is approximately the initial Alfvén crossing time of the box. The peak of the magnetic energy is at much larger scales (smaller  $k$ ) than the peak of the kinetic energy, consistent with the expectation that the kinetic energy should be contained within the Sweet-Parker sheets. Inset: decay of the total magnetic and kinetic energies. The total kinetic energy curve is much below the magnetic energy curve, and coincides with  $(\delta/L)E_M$ , in agreement with Eq. (18), with  $\delta/L$  computed as the ratio of the wavenumbers at which  $k\mathcal{E}_M(k)$  and  $k\mathcal{E}_K(k)$  peak. Bottom panel: Plot of the kinetic-energy decay exponent,  $p_K$ , against the magnetic-energy decay exponent,  $p_M$ , as measured in simulations with  $S_{n,0}^{-1/n} > 10$ . Results are in reasonable agreement with the theoretical prediction, Eq. (19) (coloured lines), and are inconsistent with  $E_K \propto E_M$  (grey line).

Eq. (18). The lower panel shows the kinetic-energy decay exponents,  $p_K$ , plotted against the corresponding exponents for the magnetic energy,  $p_M$ , confirming that a faster decay of kinetic energy is realised in our simulations, in reasonably good agreement with our theoretical prediction, Eq. (19).

We note that, while we do observe faster decay of the kinetic energy than the magnetic energy in our simulations, the difference is not as stark as in the numerical study by [9], who found  $E_K \propto E_M^2$ . As we will discuss in Section IV, this discrepancy may arise because the initial state in their study was one with equipartition between the magnetic and kinetic energies,  $U \sim B$ , unlike the  $U \ll B$  we have employed here. We will argue that when  $U \sim B$ , the conservation of cross-helicity, even though it is sign-indefinite, might play an important role in governing the decay. Simultaneously conserving magnetic helicity and *fluctuations* in the cross-helicity, under the same formalism as we are about to propose for helicity conservation in non-helical turbulence, does imply the scaling  $E_K \propto E_M^2$  conjectured in [9].

To conclude, the results of this section represent what we consider compelling evidence that helical, magnetically dominated MHD turbulence relaxes by the coalescence of magnetic structures via magnetic reconnection. Physically, this implies that the correct way to think about the system is as consisting of a collection of magnetic structures that are unable to relax under ideal dynamics due to the topological constraints imposed by the flux freezing, and, therefore, relax via coalescence on a timescale at which these constraints can be broken, i.e., on the reconnection timescale.

### III. DECAY OF NON-HELICAL TURBULENCE

Having established a theory of reconnection-controlled decay for helical turbulence, we now consider the case of non-helical turbulence, i.e., turbulence for which the volume-averaged magnetic-helicity density [Eq. (4)] vanishes. Here, as in Section II, we consider the decay from an initial state with predominant magnetic energy ( $B \gg U$ ), postponing the discussion of the case with  $U \sim B$  until Section IV E. As we have already noted, the mechanisms controlling the evolution of such turbulence are not well understood. Numerically, a power law close to  $t^{-1}$  has been measured [15, 18–20, 22], prompting comparisons with the two-dimensional decay [7, 8, 23], which conserves ‘anastrophy’, or the square of the magnetic vector potential (see Appendix A), resulting in a  $t^{-1}$  decay law independently of whether the decay is controlled by reconnection. The evidence that has been presented for this picture in three dimensions relies on demonstrating that the mean-square magnetic vector potential (defined according to some particular, necessarily non-unique gauge choice) changes more slowly with time than does the magnetic energy [22]. However, we point out that this will be true for any decay satisfying  $B^\alpha L \sim \text{const}$  for any  $\alpha > 0$ . Here, we propose a different theory of non-helical decay.

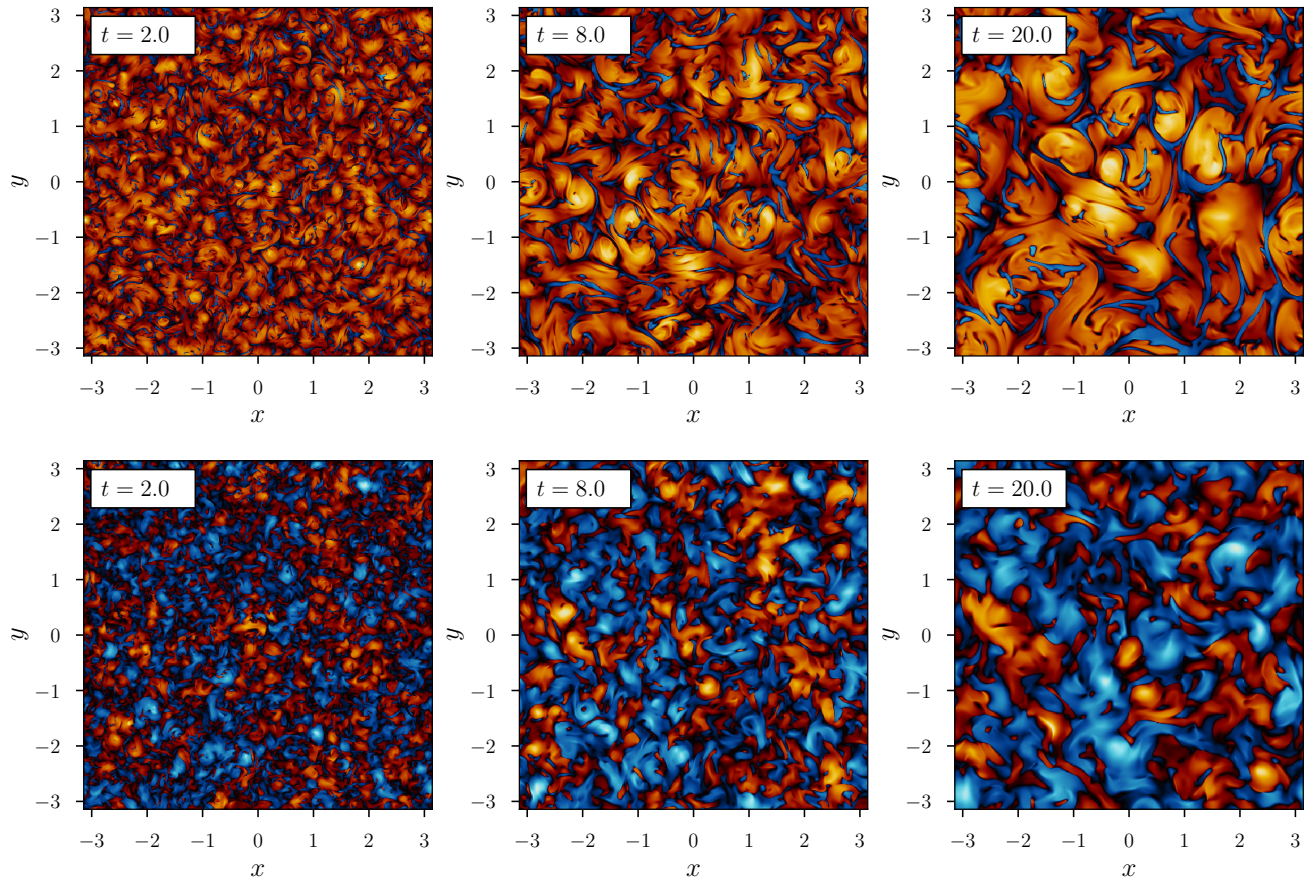


FIG. 3. Slices of  $\mathbf{B} \cdot \hat{\mathbf{J}}$ , the projection of the magnetic field onto the direction of the electric current ( $\hat{\mathbf{J}}$  is the unit vector in this direction), for three different times during helical (above) and non-helical (below) simulations with  $n = 2$ ,  $\eta_2 = 2 \times 10^{-4}$  (time is in code units, as explained in the caption to Fig. 2). Positive values are shown in red, negative values in blue.  $\mathbf{B} \cdot \hat{\mathbf{J}}$  is a local measure of the twist of the magnetic field lines, with different signs indicating different directions of the twist. It is also related to the magnetic helicity, because the sign of  $\mathbf{B} \cdot \hat{\mathbf{J}}$  is equal to the sign of the magnetic helicity for a fully-relaxed helical magnetic structure, according to the J. B. Taylor relaxation theory [37]. Indeed, our helical simulations do feature a super-abundance of blobs with positive  $\mathbf{B} \cdot \hat{\mathbf{J}}$ , while in our non-helical simulations, blobs with both signs of  $\mathbf{B} \cdot \hat{\mathbf{J}}$  have approximately equal representation.

### A. Qualitative theory of non-helical decay

The key point, already made in Section I, is that a vanishing mean helicity density does not imply that individual magnetic structures are non-helical, because helicity is not a sign-definite quantity. Moreover, if not constrained by higher-order topological invariants, non-helical magnetic structures will relax to zero energy on the ideal timescale. For example, consider a toroidal structure without a twist – such a structure will shrink under the magnetic tension force (driving outflows along its axis) to zero magnetic energy. In contrast, for a toroidal structure with a net twist relative to the poloidal axis, such a relaxation is topologically impossible. Thus, we expect a collection of helical structures of different signs to be the natural state of non-helical MHD turbulence. Indeed, visualisations of our simulations do appear to support this intuition, see Fig. 3.

To motivate the more formal approach to follow, we first present an informal ‘cartoon’ of the expected dynamics (Fig. 4). Consider a volume filled with helical magnetic structures, which we shall refer to as ‘blobs’, as we wish to remain agnostic about their precise morphology. As in the helical case, we expect that topological constraints will hinder their relaxation on ideal timescales, and that instead the blobs will evolve via coalescences with other blobs on the prevailing reconnection timescale.

For simplicity, suppose that all blobs have helicity  $\sim H$ , and for the moment, that they all have the same sign of helicity. When any two blobs merge, the resulting structure will have helicity  $H' = 2H$ , implying that the characteristic magnetic field and length scale,  $B$  and  $L$ , will satisfy  $B'^2 L'^4 \sim 2B^2 L^4$ . If every blob in the system undergoes such a pairwise merger, then the total number of blobs,  $N$ , will decrease by a factor of 2:

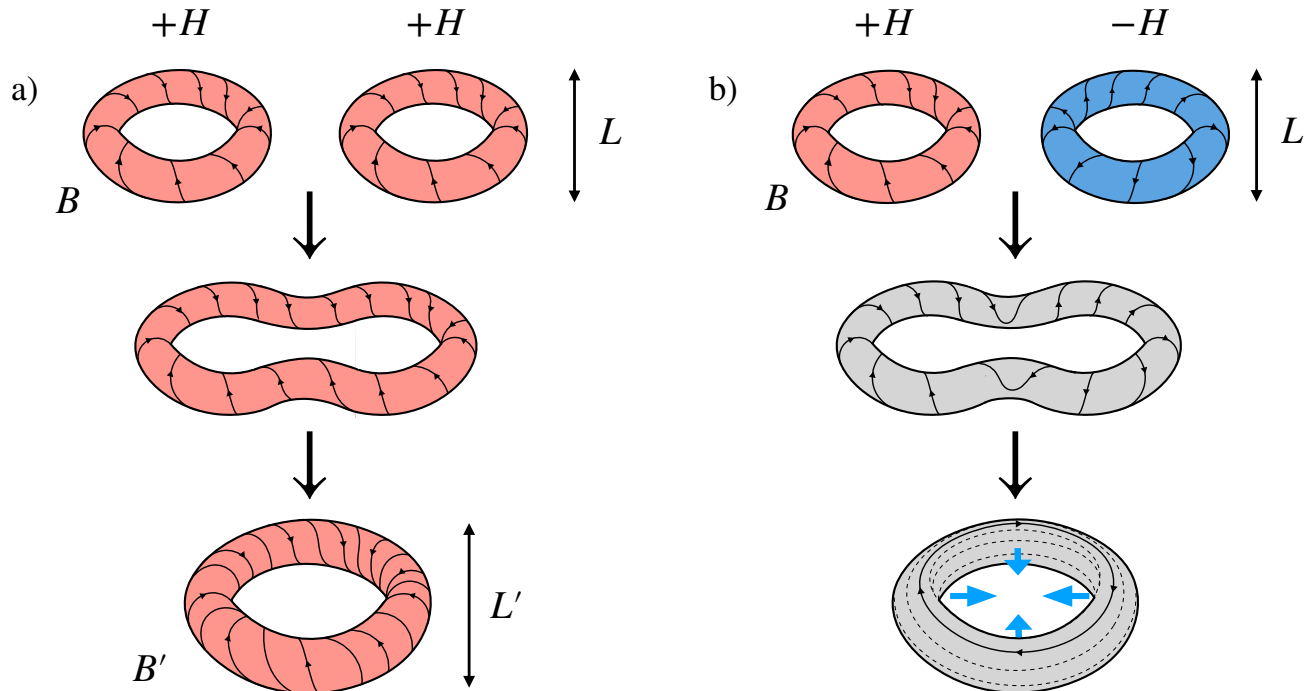


FIG. 4. (a) Cartoon of a typical merger of two helical structures ('blobs'). As explained in the main text,  $B'^2 L' = B^2 L$  for helical turbulence in which this is the only allowed process. (b) This additional 'annihilation' process is also possible in non-helical turbulence, and should occur equally frequently. The presence of this process modifies the previous scaling to  $B'^{4/5} L' = B^{4/5} L$ .

$N' = N/2$ . Assuming the blobs fill all space, their characteristic size must then increase as  $L' = 2^{1/3} L$ . Together, these relations imply  $B^2 L \sim \text{const}$ , which, of course, is precisely the condition obtained from the conservation of the volume-averaged helicity density, Eq. (9).

In contrast, for a system with vanishing total helicity, there will be an equal number of blobs with helicity  $-H$  as those with  $+H$ . When two blobs with opposite helicities merge, the resulting structure will be non-helical and, assuming that no higher-order topological invariants constrain its subsequent evolution, will relax to zero magnetic energy on the ideal timescale. In other words, when blobs of opposite helicity merge, they mutually 'annihilate'. Otherwise, the signs of the helicities of the blobs should not modify the dynamics, so the system will have no preference between like-helicity and opposite-helicity mergers. This implies that, after one merger timescale, we will have  $N' = N/4$ , because of any four randomly chosen blobs, on average, two will annihilate, and two will merge to form a single blob. Again, assuming blobs fill all space, we have  $L' = 2^{2/3} L$ , which, together with  $B'^2 L'^4 \sim 2B^2 L^4$ , implies

$$B'^{4/5} L' \sim \text{const}. \quad (21)$$

This new scaling is the non-helical analogue of Eq. (9).

This picture, while conceptually simple, does rely on significant assumptions about the nature of the dynamics

that are not obviously justifiable, e.g., that all structures have the same length scale and helicity, that the only dynamical process is mergers (rather than, say, fragmentation due to MHD instabilities) and that all mergers are pairwise processes. We now discuss how to formalise it.

## B. Formal theory of non-helical decay

We propose that the general evolution of a collection of localised structures of mixed magnetic helicity should conserve the integral

$$I_H = \lim_{V \rightarrow \infty} \int_V d^3 \mathbf{r} \langle h(\mathbf{x}) h(\mathbf{x} + \mathbf{r}) \rangle, \quad (22)$$

where, as before,  $h = \mathbf{A} \cdot \mathbf{B}$  is the helicity density, and angle brackets denote an ensemble average. The form of this integral is immediately reminiscent of the integrals that govern hydrodynamic decay: the already-introduced Loitsyansky integral, Eq. (1), and the Saffman integral [32],

$$I_P = \lim_{V \rightarrow \infty} \int_V d^3 \mathbf{r} \langle \mathbf{u}(\mathbf{x}) \cdot \mathbf{u}(\mathbf{x} + \mathbf{r}) \rangle. \quad (23)$$

The Saffman integral is somewhat more obscure than the Loitsyansky integral, because it formally vanishes for

incompressible turbulence. Physically, its conservation is related to the conservation of linear momentum,  $\mathbf{P}$ , much as the conservation of the Loitsyansky integral is related to angular-momentum conservation, and, as we are about to show,  $I_H$  is related to helicity conservation. Owing to this analogy, of which we shall make further profitable use in Section IV, we will refer to  $I_H$  as the ‘Saffman helicity invariant’. We proceed by establishing the claims that, in non-helical turbulence,  $I_H$  is gauge invariant, finite, and conserved. These arguments are in most respects analogous to those originally made by Saffman for  $I_{\mathbf{P}}$  [32] (see [5] for a review).

### 1. $I_H$ is gauge-invariant.

Assuming that volume and ensemble averages are the same,

$$I_H = \lim_{V \rightarrow \infty} \frac{1}{V} \left[ \int_V d^3\mathbf{x} h(\mathbf{x}) \right]^2 = \lim_{V \rightarrow \infty} \frac{1}{V} H_V^2, \quad (24)$$

so  $I_H$  is the density of magnetic helicity squared. Gauge invariance is then guaranteed in the same manner as for the magnetic helicity, by arranging that the surface of the volume  $V$  is always normal to the magnetic-field direction. This can always be achieved because of our assumption that the magnetic field forms localised structures, which are arbitrarily small compared to  $V$  in the limit  $V \rightarrow \infty$ .

### 2. $I_H$ is finite.

Returning to the definition of  $I_H$ , Eq. (22), and assuming that the system has no preference for accumulation of like- or opposite-helicity structures,  $\langle h(\mathbf{x})h(\mathbf{x} + \mathbf{r}) \rangle$  is zero if  $\mathbf{r}$  extends beyond the characteristic size of a helical structure,  $L$ , and of size  $\sim \langle h^2 \rangle \sim B^4 L^2$  otherwise. Formally, this requires the two-point magnetic-helicity-density correlation function to decay faster than  $r^{-3}$  as  $r \rightarrow \infty$ . This is the condition for the magnetic structures to be ‘localised’. The estimate  $\langle h^2 \rangle \sim B^4 L^2$  also requires that field structures at the energy-containing scale be maximally helical – presumably there is a tendency towards that due to faster relaxation of non-helical structures. As a consequence,  $I_H$  is finite, and is of size  $\sim B^4 L^5$ .

Another way of thinking about this is to consider the integral in Eq. (24) as a random walk in the net helicity – the number of ‘steps’ is  $V/L^3$ , so

$$H_V = \int_V d^3\mathbf{x} h(\mathbf{x}) \sim \left( \frac{V}{L^3} \right)^{1/2} B^2 L^4. \quad (25)$$

Then there is cancellation of the volume  $V$  in Eq. (24), and the scaling  $I_H \sim B^4 L^5$  is recovered.

### 3. $I_H$ is conserved.

According to Eq. (25), the expectation value of the helicity in a large volume of non-helical turbulence is  $H_V \propto V^{1/2}$ . As  $\eta \rightarrow 0^+$ , the magnetic helicity is conserved during all processes that occur locally inside the

volume  $V$ , so  $H_V$  can only be changed by processes occurring at the surface of this volume,  $S = \partial V$ . These are fluxes of helicity in or out of the volume, or else reconnection with magnetic structures not contained within the volume. However, both are random processes and hence the rate of change of helicity associated with them scales as  $\sim S^{1/2} \sim V^{1/3}$ . Ultimately, then, we find that

$$\frac{1}{H_V} \frac{dH_V}{dt} \propto V^{-1/6}, \quad (26)$$

with the result that in the limit  $V \rightarrow \infty$ ,  $H_V$  is a conserved quantity. Therefore, so is  $I_H$ .

In the context of this work, the relevance of the conservation of  $I_H$  is that it implies precisely the same scaling as we found from our qualitative theory, Eq. (21). The more formal argument proposed here is much more general, however: while it requires that helical structures be localised (i.e., that local correlations decay sufficiently quickly with distance), and that there be no preference for accumulation of like-helicity or opposite-helicity structures, it does not require that all structures be of the same size or magnitude of helicity at any given instant, and neither does it require that the only relevant dynamics be pairwise mergers. The cartoon presented in Section III A, should, therefore, be considered as a particular example of dynamics that would conserve  $I_H$ , and that, therefore, must produce the correct scaling, but not as the only dynamics allowed in the system, or required to be prevalent in order for the scaling (21) to hold.

## C. Decay laws

As regards the decay laws, Eq. (15) with  $\alpha = 4/5$ , as demanded by Eq. (21), implies a magnetic-energy decay

$$E_M \propto t^{-20/17} \simeq t^{-1.18}, \quad (27)$$

if the dynamics occur on the Sweet-Parker timescale (with Laplacian viscosity), or

$$E_M \propto t^{-10/9} \simeq t^{-1.11}, \quad (28)$$

if reconnection is fast, i.e., either stochastic or plasmoid-dominated. These exponents are both close to  $-1$ , so are consistent with previous numerical results that have reported a power law decay  $\propto t^{-1}$  [15, 18–20, 22].

For the kinetic energy, we again expect Eq. (18) to hold. Under the Sweet-Parker scalings and  $B^{4/5} L \sim \text{const}$ , this becomes

$$E_K \sim E_M^{(14n-9)/10n}. \quad (29)$$

For  $n = 2$  and  $n = 4$ , this gives  $E_K \sim E_M^{0.95}$  and  $E_K \sim E_M^{1.175}$ , respectively. The closeness of these exponents to 1 indicates that the current-sheet aspect ratio changes more slowly in the non-helical case than the helical case, and explains why no significant difference in the kinetic- and magnetic-energy decay laws has been reported in previous numerical studies.

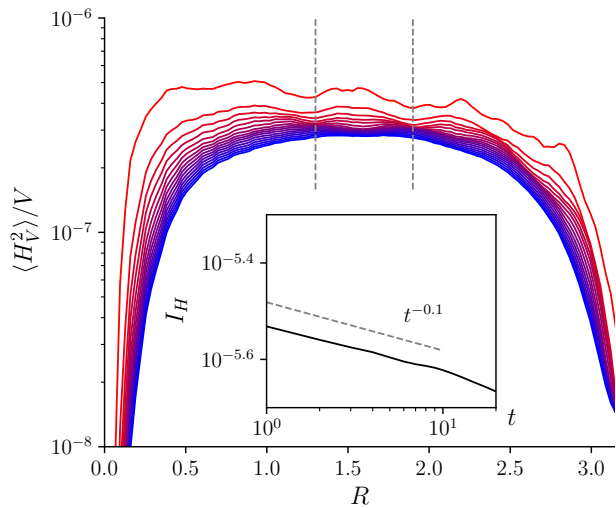


FIG. 5. Confirmation of the expected scaling of  $\langle H_V^2 \rangle / V$  with volume,  $V = (2R)^3$ , for a simulation with  $n = 6$ ,  $\eta_6 = 1.42 \times 10^{-12}$ . Flat parts of the curves correspond to the volume-independent limit, as expected by Eq. (25). Curves are plotted with a constant interval of 1.0 between  $t = 0.0$  (red) and  $t = 15.0$  (blue), where time is in code units, as explained in the caption to Fig. 2. The inset shows the evolution of  $I_H$ , computed as the mean value of  $\langle H_V^2 \rangle / V$  between  $R = 1.3$  and  $R = 1.9$ .

#### D. Numerical results

We first address the question of the scaling and conservation of  $I_H$  in our simulations. Fig. 5 shows plots of  $\langle H_V^2 \rangle / V$ , where  $V$  is a cube of width  $2R$ , and we take an ensemble average over many different cube positions in the simulation box (employing the Coulomb gauge,  $\nabla \cdot \mathbf{A} = 0$ , for numerical convenience). As  $R \rightarrow 0$ ,  $\langle H_V^2 \rangle / V \propto V \rightarrow 0$ . Similarly,  $\langle H_V^2 \rangle / V$  vanishes as  $R \rightarrow \pi$ , because then  $V$  is the entire periodic simulation domain, which has zero magnetic helicity by construction. However, for intermediate values of  $R$ ,  $\langle H_V^2 \rangle / V$  turns out to be independent of  $V$ , confirming the random-walk scaling, Eq. (25).

The value of  $I_H$  is the size of  $\langle H_V^2 \rangle / V$  in this flat region. Computing the average of  $\langle H_V^2 \rangle / V$  between the two dashed lines in Fig. 5 as a function of time, we find that  $I_H$  decays approximately as  $t^{-0.1}$  (see inset in Fig. 5). Since  $I_H \sim B^4 L^5$ , this implies a decay of  $B^{4/5} L \propto t^{-0.02}$ , i.e., this combination stays essentially constant – Eq. (21) holds well. We conclude that  $I_H$  is finite and conserved. These results should be compared to the expected evolution of  $I_H \sim B^4 L^5$  under the assumption of conservation of anastropy, as in two dimensions, and the robust Sweet-Parker scaling for  $n = 4$ , i.e.,  $BL \sim \text{const}$ ,  $B^2 \sim t^{-3/4}$  (see Appendix A), predicting growth,  $B^4 L^5 \sim t^{3/8}$ . Thus, the distinction between our theory of non-helical decay and the conjecture of quasi-two-dimensional dynamics [15, 19, 22] is measurable in numerical simulations, and there is strong evidence in

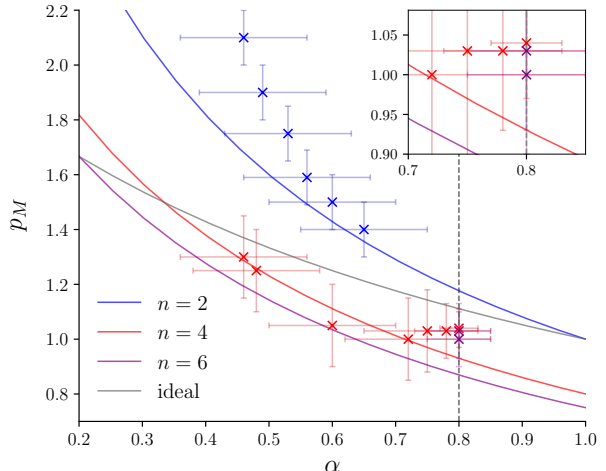


FIG. 6. Relation between the empirically obtained magnetic-energy-decay power-law exponent,  $p_M$ , and the value of  $\alpha$  for which  $B^\alpha L \sim \text{const}$  for the non-helical simulations. As in Fig. 1, solid curves show the expected relationship, Eq. (15), for decays occurring on the Sweet-Parker timescale, with  $n = 2$ ,  $n = 4$  and  $n = 6$  shown in blue, red, and magenta respectively. The grey solid curve depicts the scaling given by Eq. (12). Simulation results are in excellent agreement with the coloured curves, with better agreement as  $\alpha$  increases towards the limiting value of  $4/5$ . As in the helical case, simulations at the largest Lundquist numbers appear to be on the brink of the transition to the fast-reconnection regime. The full set of decay curves from which this plot was derived can be found in Appendix C.

support of the former over the latter.

As in the helical case, the asymptotic scaling  $B^{4/5} L \sim \text{const}$  will not necessarily be satisfied for a decay at finite  $\eta_n$ . Nevertheless, we can still measure a value of  $\alpha$  for which  $B^\alpha L \sim \text{const}$  is satisfied, and compare the measured value of the magnetic-energy decay exponent,  $p_M$ , with the one expected for a decay on Sweet-Parker or ideal timescales. The results of this comparison are shown in Fig. 6. While agreement with the Sweet-Parker curves (coloured) for  $\alpha < 4/5$  is not quite as good as in the helical case, we still observe (i) a clear preference for the Sweet-Parker prediction over the prediction of a decay on ideal timescales (grey), and (ii) convergence to  $B^{4/5} L \sim \text{const}$  for the hyper-dissipative simulations.

Let us now turn to the kinetic energy. Fig. 7 again shows that, like in the helical case, the kinetic energy is peaked at smaller scales than the magnetic energy is, consistent with the expectation of Alfvénic outflows in current sheets. We also find that Eq. (18) is very well satisfied, and a reasonable agreement with Eq. (29), although the magnetic- and kinetic-energy decay exponents are very close to each other.

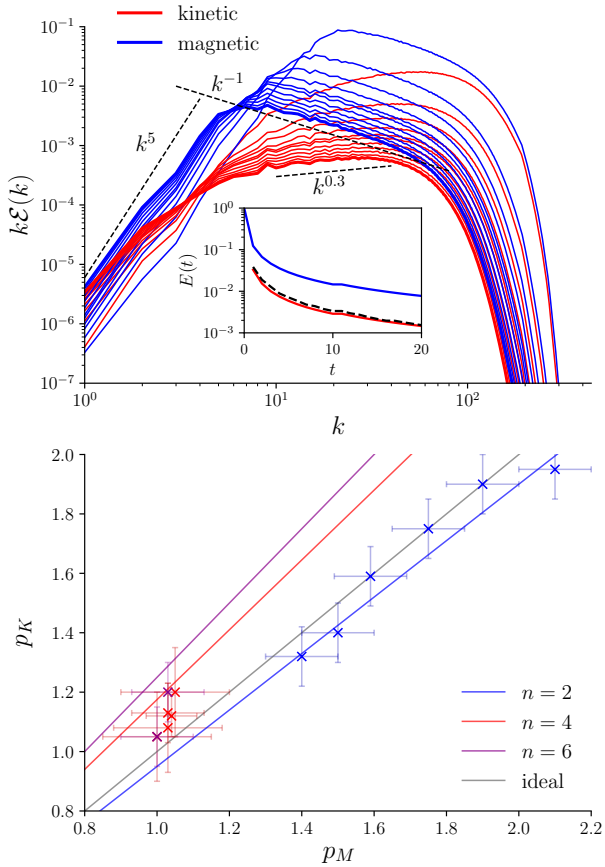


FIG. 7. Top panel: Evolution of  $k\mathcal{E}(k)$ , where  $\mathcal{E}(k)$  is the spectral energy density, for the magnetic (blue) and kinetic (red) energies. These plots are obtained from the non-helical simulation with  $n = 4$ ,  $\eta_4 = 2 \times 10^{-8}$ . Each plot of  $k\mathcal{E}(k)$  is separated by a time interval of 2.0 between  $t = 1.0$  to  $t = 21.0$  ( $t = 21.0$  in bold), where time is in code units, as explained in the caption to Fig. 2. As in the helical case (Fig. 2), the peak of the magnetic energy is at much larger scales (smaller  $k$ ) than the peak of the kinetic energy spectrum, consistent with the expectation that the kinetic energy should be contained within the Sweet-Parker sheets. Inset: decay of the total magnetic and kinetic energies. The total kinetic energy curve is much below the magnetic energy curve, and coincides with  $(\delta/L)E_M$ , in agreement with Eq. (18). Here, we compute  $\delta/L$  as the ratio of the wavenumbers at which  $k\mathcal{E}_M(k)$  and  $k\mathcal{E}_K(k)$  peak. Bottom panel: The kinetic-energy decay exponent,  $p_K$ , against the magnetic-energy decay exponent,  $p_M$ , as measured in simulations with  $S_{n,0}^{-1/n} > 10$ . Results are in reasonable agreement with the theoretical prediction, Eq. (29) (coloured lines), though as noted in the main text, this prediction is very similar to  $E_K \propto E_M$  (grey).

## IV. DISCUSSION

### A. Case of small, but non-zero, helicity

In this paper, we have proposed a way to treat helical and non-helical MHD turbulence within the same theoretical framework. Of course, no real field config-

uration will have precisely zero helicity, and therefore it is important to consider the evolution of a field configuration with small, but non-zero, magnetic helicity. In such a case, the system will undergo a transient period of evolution according to the non-helical decay law  $B^{4/5}L \sim \text{const}$  [Eq. (21)], before ultimately entering the fully helical regime, with a corresponding change in the decay law to  $B^2L \sim \text{const}$  [Eq. (9)].

This conclusion is an immediate consequence of the non-helical decay laws, as follows. Suppose that the system starts with some small helicity fraction  $\sigma_0 \ll 1$ , defined so that the total helicity is  $H = \sigma_0 B_0^2 L_0 V$ . At a later time, since helicity is conserved,

$$\sigma B^2 L = \sigma_0 B_0^2 L_0. \quad (30)$$

Because  $\sigma_0 \ll 1$ , the system is not controlled by its total helicity, at least initially. It therefore evolves according to  $B^{4/5}L \sim \text{const}$ . Using this in Eq. (30), we find

$$\sigma \sim \sigma_0 \left(\frac{B}{B_0}\right)^{-6/5} \sim \sigma_0 \left(\frac{L}{L_0}\right)^{3/2}. \quad (31)$$

Thus, the helicity fraction  $\sigma$  will grow with time. This can continue until  $\sigma \sim 1$ , at which point the system enters the helical regime. This occurs when

$$B \sim B_0 \sigma_0^{5/6}, \quad L \sim L_0 \sigma_0^{-2/3}, \quad (32)$$

provided that the energy-containing scale  $L$  has not yet reached the system size.

This result is intuitive from the cartoon picture presented in Section III: when blobs with one sign of helicity are more populous, the ultimate consequence of random mergers is for the less populous type to be used up (although this can take a long time, which scales with an appropriate negative power of  $\sigma_0$ , if the initial population imbalance is small).

The same conclusion can be reached from the consideration of the Saffman helicity invariant, Eq. (24), though some care should be taken, as  $I_H$  is formally infinite in the presence of any net helicity. However, if the helicity fraction  $\sigma$  is small, then we can interpret the limit  $V \rightarrow \infty$  in Eq. (24) as requiring  $L^3 \ll V \ll V_c$ , where  $V_c$  is the critical volume at which  $H_V$  ceases to be dominated by the net helicity fluctuation owing to its collection of helical structures of random signs, and instead is dominated by the helicity imbalance (see Fig. 8). This condition implies

$$\sigma \langle h^2 \rangle^{1/2} V_c \sim \langle h^2 \rangle^{1/2} L^3 \left(\frac{V_c}{L^3}\right)^{1/2} \implies V_c \sim \frac{L^3}{\sigma^2}. \quad (33)$$

For any  $V$  such that  $L^3 \ll V \ll V_c$ , the arguments presented in the previous section in favour of the conservation of  $H_V$  remain valid and hence  $I_H$  still provides the dominant constraint on the decay of magnetic structures. Choosing instead  $V > V_c$ ,  $\langle H_V^2 \rangle \sim \sigma^2 V B^4 L^2 \sim \text{const}$ , so

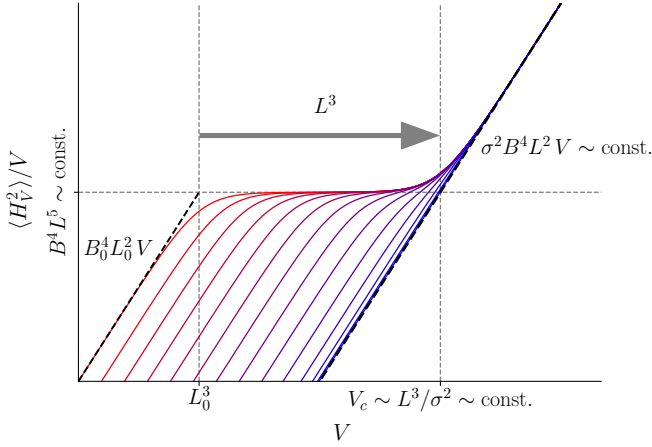


FIG. 8. Schematic of  $\langle H_V^2 \rangle / V$  as function of  $V$ , as a system with small initial fractional helicity,  $\sigma_0$ , transitions to the fully helical regime, as explained in the main text. The progression of time is shown by red  $\rightarrow$  blue, with plots at logarithmically spaced time intervals. Note that both axes are plotted on logarithmic scales.

we recover the evolution equation for  $\sigma$ , Eq. (30). However, when ultimately  $\sigma \sim 1$ , there is no longer any possibility of satisfying  $L^3 \ll V \ll V_c$ , because  $V_c \sim L^3$ . At this point,  $\langle H_V^2 \rangle \sim V B^4 L^2$  for any chosen volume, and we are back to the fully helical scaling, Eq. (9).

These arguments suggest that the non-helical decay is ultimately transient for any real system, and there will always eventually be a transition to the helical regime, provided that the growing, energy-containing scale does not reach the system size before this happens. A numerical simulation demonstrating this expected transition between the two regimes would be highly desirable, but imposes considerable numerical cost, so is left for future work.

## B. General decay principles

Let us now discuss how the principles that guided us in the above might be applied to other types of decaying turbulence. In any type of turbulence with an ideal invariant,  $F = \int d^3 \mathbf{x} f(\mathbf{x})$ , that is better conserved than the energy, the conservation of that invariant implies

$$\langle f \rangle = \lim_{V \rightarrow \infty} \frac{1}{V} \int_V d^3 \mathbf{x} f(\mathbf{x}) \sim \text{const.} \quad (34)$$

If nonlinear structures (eddies, blobs) are necessarily in possession of  $F$ , so that the characteristic size of  $f$  can be related to the sizes and correlation scales of the dynamical fields, then Eq. (34) imposes a constraint on these fields that must be satisfied as the turbulence decays. In particular, if the sign of  $f(\mathbf{x})$  within each structure is the same, either because it is sign-definite, or because the initial condition stipulates a predominance of structures of

one particular sign, then  $\langle f \rangle$  can be related to the characteristic sizes of dynamical fields and their correlation scales:

$$\langle f \rangle \sim \psi^a L_\psi^b \dots, \quad (35)$$

where  $\psi$  is a representative dynamical field,  $L_\psi$  is its correlation scale,  $a$  and  $b$  are exponents determined by the functional form of  $f$ , and ‘ $\dots$ ’ denotes the possibility of other fields and scales. Together, Eqs. (34) and (35) imply a constraint on the dynamical fields that must be satisfied during the decay,

$$\psi^a L_\psi^b \dots \sim \text{const.} \quad (36)$$

Alternatively, for sign-indefinite  $f$ , there may be no strong predominance of structures associated with either sign of the invariant. In this case,

$$\langle f \rangle \sim \sigma \langle f^2 \rangle^{1/2} \sim \sigma \psi^a L_\psi^b \dots, \quad (37)$$

where  $\sigma \ll 1$  is the fractional imbalance in  $F$ , as in Section IV A. While Eq. (34) still holds, its utility is reduced as  $\sigma$  is generally a function of time – the relationship

$$\sigma \langle f^2 \rangle^{1/2} \sim \sigma \psi^a L_\psi^b \dots \sim \text{const}, \quad (38)$$

implied by Eqs. (34) and (37), should be considered as an evolution equation for  $\sigma$ , rather than a constraint on  $\psi$  and  $L_\psi$ .

However, all is not lost. We propose that when  $\sigma \ll 1$ , conservation of *local fluctuations* in  $F$  imposes a constraint on the decay, through the associated Saffman-type integral

$$I_F = \lim_{V \rightarrow \infty} \int_V d^3 \mathbf{r} \langle f(\mathbf{x}) f(\mathbf{x} + \mathbf{r}) \rangle \sim \langle f^2 \rangle L_f^3 \sim \text{const}, \quad (39)$$

where  $L_f$  is the correlation scale of  $f$ . Again, if nonlinear structures are in possession of  $F$ , then  $\langle f^2 \rangle L_f^3$  can be related to the characteristic sizes and correlation lengths of dynamical fields,

$$\langle f^2 \rangle L_f^3 \sim \psi^c L_\psi^d \dots, \quad (40)$$

where  $c$  and  $d$  are different exponents than those in Eq. (35). Together with Eq. (39), this scaling leads to a different constraint on the decay,

$$\psi^c L_\psi^d \dots \sim \text{const}, \quad (41)$$

which is independent of the fractional imbalance  $\sigma$ .

We note that an eventual transition from the balanced regime [Eqs. (38) and (41)] to the imbalanced regime [Eq. (36)] is a general consequence of these results, because, together, Eqs. (38) and (39) imply

$$\sigma \propto L_f^{3/2}. \quad (42)$$

A necessary and sufficient condition for the fractional imbalance to grow is, therefore, that the scale  $L_f$  should increase with time. This tends to be the case for any realistic decay problem, even in the absence of inverse transfer of energy in  $k$ -space, because small-scale structures generally dissipate faster than large-scale ones.

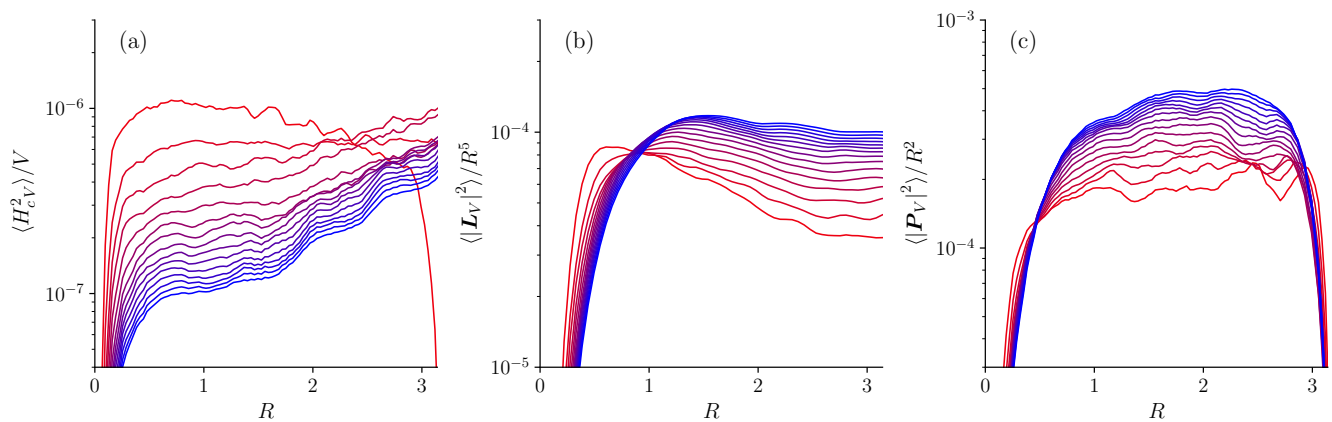


FIG. 9. Evolution of Saffman-type invariants (other than the helicity invariant) in a non-helical simulation with  $n = 6$ ,  $\eta_6 = 1.42 \times 10^{-12}$ . Curves are plotted with a constant interval of 1.0 between  $t = 1.0$  (red) and  $t = 15.0$  (blue), where time is in code units, as explained in the caption to Fig. 2. (a)  $\langle H_{cV}^2 \rangle$ , where  $H_{cV}$  is the cross-helicity contained in a cube with  $V = (2R)^3$ . While the expected random-walk scaling  $\langle H_{cV}^2 \rangle \sim V$  is obeyed,  $\langle H_{cV}^2 \rangle$  is not conserved. (b)  $\langle |\mathbf{L}_V|^2 \rangle$ , where  $\mathbf{L}_V$  is the angular momentum contained in a sphere of radius  $R$ , about the centre of the sphere. We find  $\langle |\mathbf{L}_V|^2 \rangle \sim R^5$ , in agreement with Eq. (B4). (c)  $\langle |\mathbf{P}_V|^2 \rangle$ , where  $\mathbf{P}_V$  is the linear momentum contained in a cube with  $V = (2R)^3$ . We find  $\langle |\mathbf{P}_V|^2 \rangle \sim R^2$ , in agreement with Eq. (B1).

### C. The roles of other invariants in magnetically dominated decay

The discussion in Section IV B relied on two conditions: (i) that the invariant,  $F$ , is conserved, i.e., that its rate of change is smaller than the energy decay rate, and (ii) that it can always be considered the case that typical structures possess  $F$ , so that  $\langle f \rangle$  and  $\langle f^2 \rangle$  may be related to the sizes and correlation lengths of the dynamical fields, via Eqs. (35), (37) and (40). Establishing whether (i) and (ii) holds for any given turbulent system requires some physical idea of the decay dynamics. In this section, we illustrate this point with examples from our study of magnetically dominated turbulence.

Whether a particular ideal invariant is better conserved than energy as turbulence decays depends on the decay dynamics, as different dynamical processes may result in invariants being dissipated at different rates. As an example, consider the cross-helicity,  $H_c = \int d^3\mathbf{r} \mathbf{u} \cdot \mathbf{B}$ , which is an ideal invariant of the (incompressible) MHD equations. During the decay of magnetically dominated turbulence via reconnection, cross-helicity is not conserved, because formally its decay rate has the same scaling with the dissipation coefficients  $\eta_n$  (resistivity) and  $\nu_n$  (viscosity) as the magnetic energy does. This is shown in Fig. 9(a), where we plot the average value of the squared total cross-helicity contained in a cube of volume  $V = (2R)^3$ , in a manner analogous to Fig. 5 for the magnetic helicity. We find that, while  $\langle H_{cV}^2 \rangle \sim V$ , as is expected from the random-walk argument, the associated Saffman-type invariant,  $I_{H_c}$ , which is given by the value of  $\langle H_{cV}^2 \rangle / V$  in the flat region of Figure 9(a), decays. Despite this, there are reasons to believe that cross-helicity (or its Saffman-type-invariant counterpart) might be conserved by the decaying turbulence of inter-

acting nonlinear Alfvén waves, as we will explain in Section IV D.

Dynamical processes may also govern whether structures possess the relevant invariants, condition (ii). For example, we have argued that in decaying MHD turbulence, non-helical magnetic structures tend to relax to zero energy, so that at any given time, individual magnetic structures are maximally helical. In contrast, the irrotational nature of reconnection outflows means that the Loitsyansky integral,  $I_L$ , is small for magnetically-dominated turbulence, and, therefore, does not constrain the decay. This statement is confirmed by Fig. 9(b), where we plot  $\langle |\mathbf{L}_V|^2 \rangle$  against  $R$ , where  $\mathbf{L}_V$  is the total angular momentum contained in a spherical control volume  $V$  of radius  $R$ , about its centre. A spherical control volume is chosen so as to be consistent with the derivation of the expected scaling,  $\langle |\mathbf{L}_V|^2 \rangle \sim R^5 \sim V^{5/3}$ , explained in Appendix B [Eq. (B4)]. Fig. 9(b) shows that this scaling is indeed realised in our simulations, confirming that flow structures in our simulations are irrotational, so that the Loitsyansky integral does not impose a constraint on their decay.

Finally, in Fig. 9(c), we check that  $\langle |\mathbf{P}_V|^2 \rangle \propto R^2$ , so that  $I_P$  formally vanishes, as expected. As argued in Appendix B, no conservation law can be associated with the momentum fluctuation  $\langle |\mathbf{P}_V|^2 \rangle \propto R^2$ , because the momentum inside the volume obeys the same scaling with  $R$  as the flux of linear momentum at the boundary does. Therefore,  $\langle |\mathbf{P}_V|^2 \rangle$  is not conserved, as is clear from Fig. 9(c).

As a final general remark, we point out that it is possible for nonlinear structures to possess more than one invariant. If the constraints implied by the conservation of these invariants are not mutually exclusive, then they must be satisfied simultaneously. If, however, these con-

ditions are contradictory, then it will be necessary for some of them to be broken. In that case, the decay cannot take place on the characteristic nonlinear timescale, but must instead take place on the timescale on which the weaker constraint (in the sense of quality of conservation) can be broken. This is precisely the situation in magnetically dominated turbulence: magnetic helicity is not the only topological invariant associated with the magnetic field [38], and in principle all higher-order topological invariants might impose constraints on the decay. Conserving all topological invariants is not consistent with a decay in the magnetic energy, however, because it implies  $B \sim \text{const}$ . Therefore, the decay can only proceed on the timescale on which the higher-order topological constraints may be violated, i.e., the reconnection timescale [35]. This is illustrative of a general rule that stronger, consistent constraints set the scalings between the integral scales and energies that control the decay, while inconsistent constraints set the decay timescale.

#### D. Decay of MHD turbulence in the presence of strong mean field

In this work, we have considered the relaxation of isotropic MHD turbulence, i.e., one without a mean magnetic field. The case of turbulence with a strong mean field is fundamentally different, because then the magnetic helicity is not a conserved quantity. Formally, this is because the mean field ‘sticks out’ of any volume for which one might choose to compute the magnetic helicity. Intuitively, also, this is a different situation compared to isotropic turbulence, because the constraints imposed by topology are much reduced. For example, purely magnetic structures need not persist until they are able to reconnect with each other, instead they can relax by decomposing themselves into Alfvén waves travelling in opposite directions along the mean field.

Aside from energy, MHD turbulence with a strong mean field (described by the ‘reduced MHD’ equations [39, 40]) has only one conserved quantity related to the presence of the magnetic field, the cross-helicity,

$$H_c = \int d^3\mathbf{r} \mathbf{u}_\perp \cdot \mathbf{b}_\perp, \quad (43)$$

where  $\mathbf{u}_\perp$  is the fluid velocity perpendicular to the mean magnetic field, and  $\mathbf{b}_\perp$  is the magnetic-field perturbation. Like magnetic helicity, the cross-helicity is sign-indefinite. In simulations of driven MHD turbulence with a strong mean field, a tendency to develop patches of strong local cross-helicity is observed, even in so-called balanced turbulence where the volume-averaged cross-helicity density is zero [41]. The reason for this is that structures of large cross-helicity are also structures containing strong imbalance in the sizes of the two Elsässer fields,  $\mathbf{Z}^\pm = \mathbf{u}_\perp \pm \mathbf{b}_\perp$ . Importantly, individual Elsässer fields each represent exact nonlinear solutions

to the MHD equations. Nonlinearity, and hence turbulent decay, can, therefore, only be present where both fields are present. Since  $\mathbf{u}_\perp \cdot \mathbf{b}_\perp = (|\mathbf{Z}^+|^2 - |\mathbf{Z}^-|^2)/4$ , a small cross-helicity density indicates balance between the Elsässer fields, and, therefore, large nonlinearity. Such structures are prone to turbulent decay. In contrast, structures with strong cross-helicity of either sign have reduced nonlinearity and, therefore, are more immune to turbulent decay.

All this motivates us to conjecture that decaying, balanced, reduced MHD turbulence might be controlled by the ‘Saffman cross-helicity invariant’

$$I_{H_c} = \lim_{V \rightarrow \infty} \int_V d^3\mathbf{r} \langle h_c(\mathbf{x}) h_c(\mathbf{x} + \mathbf{r}) \rangle, \quad (44)$$

where  $h_c = \mathbf{u}_\perp \cdot \mathbf{b}_\perp$ . We note that, like  $I_H$ ,  $I_{H_c}$  is an example of an invariant that depends on a fourth-order correlation function. The relevance of fourth-order correlators to the decay of MHD turbulence has previously been suggested by [42], based on the numerical results of [43].

One might expect  $I_{H_c}$  to be finite and conserved by precisely the same arguments as we presented for  $I_H$ , the Saffman helicity invariant, in Section III. By a random-walk argument analogous to the one in Section IIIB, we have

$$I_{H_c} \sim b_\perp^2 u_\perp^2 l_\perp^2 l_\parallel, \quad (45)$$

where  $l_\parallel$  and  $l_\perp$  are the characteristic lengthscales parallel and perpendicular to the mean field, respectively. For Alfvénic motions,  $b_\perp \sim u_\perp$ . Note that this scaling is on much firmer ground in the mean-field case than the isotropic case, because of the absence of topological constraints associated with helicity conservation. The parallel and perpendicular length scales can be related to each other by the conjecture of critical balance [34], which states that  $b_\perp/l_\perp \sim B_0/l_\parallel$ , and is a cornerstone of the theory of strong MHD turbulence [44, 45]. Critical balance is essentially a statement of causality: the characteristic parallel length scale of an eddy cannot be longer than the distance travelled by an Alfvén wave in one nonlinear timescale. It has been confirmed numerically to great precision in driven RMHD turbulence [46], and appears to be satisfied in decaying turbulence too [34].

Putting these scalings together, we find that  $I_{H_c} \propto b_\perp^3 l_\perp^3$ . If  $I_{H_c}$  is indeed conserved in decaying MHD turbulence, this implies

$$b_\perp l_\perp \sim \text{const}. \quad (46)$$

Then, since the energies of the Elsässer fields are comparable in balanced turbulence, the turbulent decay would likely be governed by

$$\frac{dE_{Z^\pm}}{dt} \sim -\frac{Z^\mp E_{Z^\pm}}{l_\perp} \sim E_{Z^\pm}^2. \quad (47)$$

This results in a decay of both magnetic and kinetic energy

$$E_M \sim E_K \sim t^{-1}. \quad (48)$$

Intriguingly, this decay law has indeed been observed in simulations of decaying, balanced MHD turbulence, though was rationalised differently, by assuming local effective conservation of anastrophy, which also implies Eq. (48), as in two-dimensional MHD turbulence [34] (see Appendix A).

If indeed the decay of MHD turbulence in the presence of a strong mean field conserves cross-helicity, any initial imbalance will eventually lead to a final state with maximal cross-helicity, i.e., a pure Elsässer state, according to the general argument presented in Section IV B [see Eq. (42)]. Such a state will not decay, since it is an exact solution of the non-linear RMHD equations. Such behaviour has indeed been reported in numerical studies [2, 47–49].

### E. Decay of isotropic MHD turbulence from an initial state with $U \sim B$

Another problem to which the formalism developed here may be usefully applied is to isotropic MHD turbulence decaying from an initial state with  $U \sim B$ , as opposed to the  $B \gg U$  that we have so far considered here. Such a state is the natural final state of the MHD dynamo (see, e.g., [50, 51] for reviews). In such a case, we conjecture that the simultaneous conservation of magnetic helicity *and* cross-helicity might be respected by the decay, as the constraints they imply are not mutually exclusive. Naturally, checking this conjecture will require a detailed numerical study, which is left for future work. However, the consequences of this conjecture merit discussion here, because they do appear to be consistent with other numerical studies (also, see the discussion of fourth-order correlation functions in [42]).

Let us consider a system that, as a result of dynamo or some other process, has reached equipartition between magnetic and kinetic energy,  $U \sim B$ , with the same integral scale.

#### 1. Helical magnetic field

First, let us assume that the magnetic field is helical, but that there is no predominance of either sign of cross-helicity. Then the conjecture of simultaneous conservation of magnetic helicity and cross-helicity (the latter as a Saffman-type invariant) implies  $B^2 L \sim \text{const}$  [Eq. (9)] and  $B^2 U^2 L^3 \sim \text{const}$ , respectively. Together, these conditions imply  $U \sim B^2$ , or

$$E_K \sim E_M^2 \quad (49)$$

precisely the condition found numerically by [9, 11], though without theoretical justification. They conjectured that the decay should take place on the timescale associated with the  $\mathbf{u} \cdot \nabla \mathbf{u}$  nonlinearity in the MHD equations, i.e.,  $L/U$ , which is consistent with the idea

that the timescale associated with the magnetic nonlinearity  $\mathbf{B} \cdot \nabla \mathbf{B}$  is effectively lengthened by topological constraints on the magnetic field. It is readily verified that such a decay leads to the power laws

$$E_K \sim t^{-1}, \quad E_M \sim t^{-1/2}, \quad (50)$$

as found numerically by [9, 11, 14].

The more rapid decay in kinetic energy will result in a state with  $U \ll B$ . Denoting the small perturbations to the newly established strong magnetic field by  $\delta B \sim U$ , the system should then decay in the strong-field regime, described in Section IV D. According to Eq. (48), we should then have  $\delta B^2 \sim U^2 \sim t^{-1}$ , assuming a critically balanced decay. Meanwhile,  $B^2$  should decay according to the reconnection-controlled law, either  $t^{-2/3}$  for fast reconnection, or  $B^2 \sim t^{2n/(5n-3)}$  [Eq. (16)] for Sweet-Parker reconnection. For the  $n = 4$  simulations employed by [9, 11], this implies

$$E_K \sim t^{-1}, \quad E_M \sim t^{-8/17}, \quad (51)$$

which will persist until the Sweet-Parker outflows dominate the kinetic energy, at which point the kinetic energy law should change to the one given by Eq. (19), which, independently of the type of reconnection, is always slower than  $t^{-1}$ .

The decay laws given by Eq. (51) are very close to those of Eq. (50), and, therefore, either might explain the laws found numerically by [9, 11]. Regardless, a more rapid decay of the kinetic than magnetic energy appears to be robust, as does the corresponding establishment of magnetically dominated state. Indeed, a magnetically dominated final state was observed in the simulations of [29], despite being initialised with  $U \gg B$ , with decay laws similar to Eq. (50) in the transient  $U \sim B$  regime.

#### 2. Non-helical magnetic field

Alternatively, let us consider the case of a non-helical magnetic field, initially in equipartition with the kinetic energy. Then, instead of the condition  $B^2 L \sim \text{const}$ , we have  $B^{4/5} L \sim \text{const}$  [Eq. (21)]. Together with the constraint implied by the conservation of the Saffman cross-helicity invariant,  $B^2 U^2 L^3 \sim \text{const}$ , this implies  $U \sim B^{1/5}$ , or

$$E_K \sim E_M^{1/5}. \quad (52)$$

Unlike Eq. (49), Eq. (52) implies a much faster decay of the magnetic energy than the kinetic energy. However, this decay will be short lived, because the magnetic energy can be maintained at a small, but finite, fraction of the kinetic energy by dynamo. Nonetheless, the magnetic field will always remain just below dynamical strength, because if it were to grow to dynamical levels, cross- and magnetic helicity conservation would force it to rapidly decay.

In the absence of a dynamical-strength magnetic field, the kinetic energy should decay according to the purely hydrodynamic law,  $E_K \sim t^{-10/7}$  [Eq. (3)]. Because the magnetic energy is tied to a finite fraction of the kinetic energy by the competing effects of dynamo and simultaneous cross- and magnetic-helicity conservation, it must also be the case that  $E_M \propto t^{-10/7}$ , i.e.,

$$E_M \propto (\text{but } <) E_K \sim 10^{-10/7}. \quad (53)$$

Such a decay of  $E_M$  and  $E_K$  has indeed been observed in non-helical simulations (though initialised with  $U \gg B$ ), by [22], together with evidence of dynamo action. We note, however, that it is possible that the reason  $E_M$  never grew to equipartition in these simulations was, rather, that the efficiency of the dynamo was reduced in the absence of the mean-field dynamo effect associated with helical velocity fields (see [50] and references therein).

The arguments presented in this section, if correct, suggest a remarkable general principle: an initially helical velocity field will, due to its tendency to grow a helical magnetic field through mean-field dynamo action, eventually decay in a magnetically dominated state, with  $E_M, E_K \propto t^{-2/3}$  (in the fast reconnection regime). In contrast, non-helical velocity fields will always remain in a kinetic-energy-dominated state, with  $E_M, E_K \propto t^{-10/7}$ .

In summary, the Saffman-type-invariant approach appears to be an extremely useful tool for describing the decay of turbulence subject to the conservation of sign-indefinite invariants. There are many different types of fluid turbulence to which this approach may be usefully applied – a number of them are reviewed in [5], and there are likely to be others, especially in a large variety of plasma systems increasingly of interest in the context of various types of space or astrophysical turbulence (see, e.g., [52–54]). In the physical systems where frozen-in magnetic fields are dominant actors in the dynamics, magnetic reconnection is likely to be the key physical process whereby the decay occurs. Marrying this insight to the constraints imposed by invariants appears to be a winning strategy for constructing decay theories, as it has proven to be in the MHD turbulence regimes that we have considered above.

## ACKNOWLEDGMENTS

We are grateful to N. F. Loureiro, F. Rincon, D. Uzdensky, and M. Zhou for discussions of this work. D.N.H. was supported by a UK STFC studentship. The work of A.A.S. was supported in part by the UK EPSRC grant EP/R034737/1. This work used the ARCHER UK National Supercomputing Service (<http://www.archer.ac.uk>).

## Appendix A: Decay of two-dimensional turbulence

In this appendix, we review the problem of decaying two-dimensional MHD turbulence, which, like its three-dimensional counterpart, respects the conservation of an invariant associated with the topology of the magnetic field: the square of the magnetic vector potential,  $\langle A^2 \rangle = \langle A_z^2 \rangle$ , sometimes called ‘anastrophy’. In two dimensions, anastrophy is well defined (i.e., not gauge-dependent), and evolves according to

$$\begin{aligned} \left| \frac{d}{dt} \int_V d^2\mathbf{r} A^2 \right| &= 2\eta_n \left| \int_V d^2\mathbf{r} \mathbf{A} \cdot \nabla^n \mathbf{A} \right| \\ &= 2\eta_n \left| \int_V d^2\mathbf{r} \mathbf{B} \cdot \nabla^{n-2} \mathbf{B} \right| \\ &\sim \frac{dE_M}{dt} \delta_\eta^2. \end{aligned} \quad (A1)$$

where  $dE_M/dt = \eta_n \int d^2\mathbf{r} \mathbf{B} \cdot \nabla^n \mathbf{B}$  is the rate of magnetic-energy decay due to Ohmic heating. Eq. (A1) implies that

$$\frac{d \log \int_V d^2\mathbf{r} A^2}{dt} \sim \frac{\delta_\eta^2}{L^2} \frac{d \log E_M}{dt}, \quad (A2)$$

which is an even slower rate of change than the one we found for the magnetic helicity in three dimensions, Eq. (8). Therefore, like helicity, anastrophy in two dimensions should be conserved as the turbulence decays, for  $\eta_n \rightarrow 0^+$ . Physically, anastrophy conservation is related to the conservation of in-plane magnetic flux [23]. Unlike helicity, though, the anastrophy is manifestly positive definite, so there is only one decay regime, and no Saffman-type invariant.

The conservation of anastrophy implies

$$BL \sim \text{const}, \quad (A3)$$

i.e.,  $\alpha = 1$  in Eq. (10). According to Eqs. (12) and (15), this implies a power law decay of the magnetic energy

$$E_M \sim t^{-1}, \quad (A4)$$

if the decay proceeds on the ‘ideal’  $L/B$  timescale, and

$$E_M \sim t^{-2n/(3n-2)}, \quad (A5)$$

for a decay proceeding on the Sweet-Parker timescale,  $(L/B) S_n^{1/n}$ . Coincidentally, these laws are the same for  $n = 2$ . Remarkably, the Sweet-Parker scaling for the kinetic-energy decay also turns out to be

$$E_K \sim \frac{\delta}{L} E_M \sim E_M^{(3n-2)/2n} \sim t^{-1}, \quad (A6)$$

which is independent of  $n$ . These results mean that a decay on ideal timescales produces indistinguishable power laws ( $E_K \sim E_M \sim t^{-1}$ ) to a decay on the  $n = 2$  Sweet-Parker timescale. It is perhaps for this reason that over thirty years separates the derivation of the ideal decay

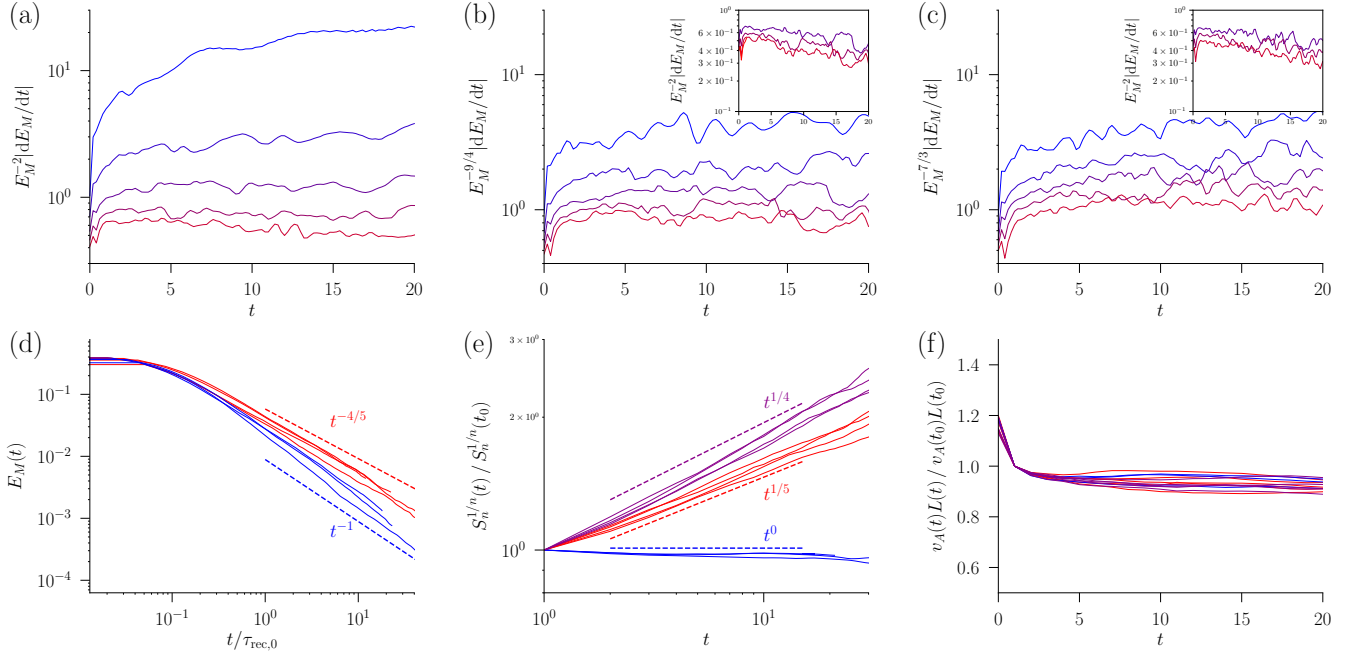


FIG. 10. Evolution of average quantities during our two-dimensional simulations. (a) Normalised energy-decay rate for  $n = 2$ , (b)  $n = 4$ , (c)  $n = 6$ . In each case, a flat profile indicates agreement with the expected decay power laws, which are  $t^{-1}$ ,  $t^{-4/5}$  and  $t^{-3/4}$ , respectively [Eq. (A5)]. Blue  $\rightarrow$  red indicates increasing  $S_n^{1/n}$ . Insets show the scaling that would be expected if the ideal law  $E_M \sim t^{-1}$  were satisfied [Eq. (A4)]. (d) Magnetic energy evolution for  $n = 2$  (blue) and  $n = 4$  (red) plotted against time renormalised to the reconnection timescale at  $t = 1$ , as in [23]. (e) Growth of the hyper-Lundquist number with time, for  $n = 2$  (blue),  $n = 4$  (red), and  $n = 6$  (magenta) simulations. Dashed lines indicate the expected scalings. (f) Constancy of  $BL$  with time. N.B. the two  $n = 2$  runs with smallest  $S_n^{1/n}$  are not plotted in (d), (e), (f) as they do not exhibit constant  $BL$  (see Table I).

law [7, 8] and the suggestion of a reconnection-controlled decay by [23]. The picture presented in [23] is analogous to (and has inspired) the ‘cartoon’ model that we proposed in Section III, although we observe that, as for the cartoon model in our study, the formulation based on the conservation of integral invariants, with decay proceeding on the reconnection timescale, is more general, as it does not require that pairwise mergers between structures of equal anisotropy (or helicity) be the only allowed dynamical process.

As a consequence of the degeneracy in power laws, it was confirmed in [23] that the Sweet-Parker timescale governed the decay in their simulations by showing that their evolution curves collapsed onto each other when time was renormalised by the initial Sweet-Parker reconnection timescale. An alternative method by which the Sweet-Parker-controlled decay can be established is via the use of hyper-dissipation, in the same manner as we have done in the main part of this work, thanks to hyper-dissipation lifting the power-law degeneracy. For example, from Eq. (A5), the magnetic-energy-decay power laws are  $t^{-4/5}$  and  $t^{-3/4}$  for  $n = 4$  and  $n = 6$ , respectively.

In Fig. 10(a-c), we show the evolution of the magnetic-energy decay rate in our two-dimensional simulations,

normalised by the power of the energy to which it is proportional in the reconnection-based theory [i.e., the power of  $B^2$  on the right hand side of Eq. (14), with  $\alpha = 1$ ]. As explained in Appendix C (also, see [9]), such plots are preferable to more conventional plots of  $\log E_M$  against  $\log t$ , because they give an unbiased estimate of the decay law. On these plots, horizontal curves indicate agreement with theoretical expectations. As the resistivity decreases, and hence the Lundquist number increases, Figs. 10(a-c) show increasingly horizontal curves, in agreement with Eq. (A5). The insets to these figures show the scaling that would be expected if the decay proceeded via ideal motions [7, 8]. In both cases, we find clearly decreasing curves for the largest Lundquist numbers tested, so these results are inconsistent with the ‘ideal’ law, Eq. (A4).

In Fig. 10(d) we show  $E_M$  against  $t/\tau_{\text{rec},0}$ , where  $\tau_{\text{rec},0}$  is the Sweet-Parker timescale  $S^{1/2}L/B$  at the start of the self-similar decay period, which we take to occur at  $t = 1$  in all cases for the purposes of this calculation. While such plots are not well-suited to an accurate determination of the decay law, they do show a clear difference in behaviour between the case of Laplacian dissipation ( $n = 2$ , blue) and hyper-dissipation ( $n = 4$ , red). As previously mentioned, the collapse of the de-

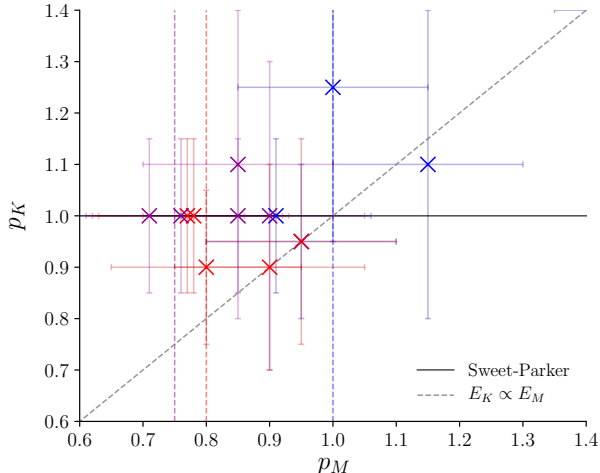


FIG. 11. Relation between the measured magnetic- and kinetic-energy decay exponents in our two-dimensional simulations. Eq. (A6) predicts that all simulations should have  $p_K = 1$ , independently of  $p_M$ . While many of the simulations do fall close to this line, the evidence for  $p_K = 1$  over  $p_K = p_M$  is not very strong, owing to the closeness of all powers involved, and the large amount of noise in the two-dimensional simulations (see end of Appendix A).

cay curves onto each other under such a normalization was presented as evidence for a reconnection-controlled decay in two-dimensions by [23]. Fig. 10(d) shows that the same behaviour occurs in the  $n = 4$  hyper-dissipative case, and we find the same in the  $n = 6$  case (not shown), so we agree entirely with [23] that the decay is controlled by reconnection.

The remaining panels of Fig. 10 show other relevant quantities besides the magnetic energy. In Fig. 10(e), we show the evolution of the hyper-Lundquist number, which is in excellent agreement with theoretical expectations based on Eqs. (A3) and (A5). Interestingly, the hyper-Lundquist number is expected to grow when  $n > 2$ , so even if the simulation starts in the Sweet-Parker reconnection regime, it can ultimately transition to the plasmoid-dominated regime. We reiterate that in such a regime, while formidable to simulate, the reconnection timescale becomes proportional to the ideal timescale (though shorter by a factor of  $10^{-2}$  [24]), and then we expect a transition to the ‘ideal’  $t^{-1}$  decay [Eq. (A4)]. Finally, Fig. 10(f) confirms that  $BL$  is indeed constant during the decay, as demanded by the conservation of anastrophy.

Consider now the decay of the kinetic energy. Fig. 11 shows plots of our best numerical estimates of  $p_K$  vs.  $p_M$ . While we note that most of our runs do fall close to the  $p_K = 1$  line, as predicted by (A6), the numerical evidence for  $p_K = 1$  over  $p_K = p_M$  is not very strong, due to the similarity between the decay laws involved. Another factor that makes this comparison difficult is the

high level of noise in the decay curves (see Fig. 14), which is not present in three dimensions, and arises because of the greatly reduced number of magnetic structures in the two-dimensional simulations. Because we initialise both types of simulation with the magnetic-spectral-energy density peaked at the same wavenumber,  $k_p \simeq 33$  (see Appendix C), there are initially  $\sim 33$  times fewer structures in our two-dimensional runs.

## Appendix B: Random-walk scalings for Loitsyansky and Saffman integrals

In this appendix, we consider the status of the Loitsyansky and Saffman integrals [Eqs. (1) and (23), respectively] in the formalism that we put forward in Section IV B, because, in fact,  $\langle |\mathbf{L}_V|^2 \rangle$  and  $\langle |\mathbf{P}_V|^2 \rangle$  do not scale with  $V$  as suggested by the naïve random-walk estimates employed in Section III B, owing to the reasons we now discuss.

First, let us consider  $\langle |\mathbf{P}_V|^2 \rangle$  for a volume  $V \sim R^3$ . The random-walk argument put forward in Section III B suggests that  $\langle |\mathbf{P}_V|^2 \rangle \propto R^3$  [5, 32]. However, owing to incompressibility, the correct scaling turns out to be

$$\begin{aligned} \langle |\mathbf{P}_V|^2 \rangle &= \left\langle \left[ \int_V d^3 \mathbf{x} \mathbf{u} \right]^2 \right\rangle = \left\langle \left[ \int_S d\mathbf{S} \times \boldsymbol{\psi} \right]^2 \right\rangle \\ &\sim L^4 U^2 R^2, \end{aligned} \quad (\text{B1})$$

where  $\mathbf{u} = \nabla \times \boldsymbol{\psi}$ , and we have used the fact that  $\int_S d\mathbf{S} \times \boldsymbol{\psi}$  will sum as a random walk. Therefore, the Saffman integral,

$$I_P = \lim_{V \rightarrow \infty} \langle |\mathbf{P}_V|^2 \rangle / V \rightarrow 0 \quad (\text{B2})$$

for incompressible turbulence. Note also that the linear-momentum fluctuation in  $V$  will not be conserved, because it is formally the same size,  $\propto R$ , as the net surface flux that can cause it to change. Therefore, linear-momentum conservation generally does not control decaying, incompressible turbulence. For the same reason, the conservation of the total magnetic flux  $\int d^3 \mathbf{x} \mathbf{B}$  also does not provide a constraint on the decay of MHD turbulence.

However, it turns out that, for sufficiently large volumes, these seemingly innocuous local fluctuations in the linear momentum actually dominate  $\langle |\mathbf{L}_V|^2 \rangle$ , instead of the local rotation of the eddies. The reason is that structures further from the origin will contribute more angular momentum than closer structures. For irrotational flow structures, it turns out that  $\langle |\mathbf{L}_V|^2 \rangle \sim R^5$ , owing to this effect. This conclusion can be obtained from a random-walk argument: the expected square angular momentum in a spherical shell of radius  $r$ , with width  $\delta r$  satisfying  $L \ll \delta r \ll r$ , is

$$\delta \langle |\mathbf{L}|^2 \rangle \sim r^2 U_t^2 L^6 \frac{4\pi r^2 \delta r}{L^3}, \quad (\text{B3})$$

where  $U_t$  is the typical size of the net translational velocity of a structure. Assuming any two shells are uncorrelated, the total square angular momentum is simply the sum over all shells of Eq. (B3). Integrating over  $r$ , we get

$$\langle |\mathbf{L}_V|^2 \rangle \sim U_t^2 L^3 R^5. \quad (\text{B4})$$

In fact, the scaling Eq. (B4) may also be adjusted by incompressibility. This is because

$$\mathbf{L}_V = \int_V d^3\mathbf{x} \mathbf{x} \times \mathbf{u} = \int_V d^3\mathbf{x} \mathbf{x} \times (\nabla \times \boldsymbol{\psi}). \quad (\text{B5})$$

Integrating by parts and expanding the double cross product gives

$$(\mathbf{L}_V)_i = \int_{\partial V} dS \left( \delta_{ij} - \frac{r_i r_j}{r^2} \right) r \psi_j - 2 \int_V d^3\mathbf{x} \psi_i. \quad (\text{B6})$$

Since  $\boldsymbol{\psi}$  is a random field, the first integral scales as  $R^2$ , so it dominates over the second, which scales as  $R^{3/2}$ . Therefore, Eq. (B6) implies

$$\langle |\mathbf{L}_V|^2 \rangle \sim U_t^2 L^4 R^4. \quad (\text{B7})$$

Whether ultimately Eq. (B4) or Eq. (B7) provides the correct scaling turns out to depend on the strength of long-range correlations between eddies. In flows where individual eddies have significant linear momentum, the far-field velocity associated with a given eddy turns out to be  $\mathbf{u}_\infty \propto r^{-3}$ , so  $\boldsymbol{\psi}_\infty \propto r^{-2}$ , which decays sufficiently slowly with  $r$  to violate the random-walk scaling in Eq. (B6). In such cases,  $\langle |\mathbf{L}_V|^2 \rangle \sim R^5$ , in agreement with Eq. (B4). In contrast, in flows where individual eddies are angular-momentum dominated (which is the regime in which one might expect angular momentum conservation to impose a constraint on the decay), it turns out that  $\mathbf{u}_\infty$  decays faster than  $r^{-3}$ , so Eq. (B7) results. A formal derivation of these statements may be found in [5].

In either case, the scaling of  $\langle |\mathbf{L}_V|^2 \rangle$  is different to the naïve expectation,  $\langle |\mathbf{L}_V|^2 \rangle \sim R^3$ , which assumes all eddies to have no translational motion. In that case, the angular momentum of an eddy at a distance  $r$  from the origin is  $\sim [(r+L)U_r - (r-L)U_r]L^3 \sim U_r L^4$ , where  $U_r$  is the typical rotational velocity of a structure. Then Eq. (B3) becomes

$$\delta \langle |\mathbf{L}|^2 \rangle \sim U_r^2 L^8 \frac{4\pi r^2 \delta r}{L^3}, \quad (\text{B8})$$

whence

$$\langle |\mathbf{L}_V|^2 \rangle \sim U_r^2 L^5 R^3. \quad (\text{B9})$$

The stronger-than- $R^3$  scalings in (B4) and (B7) do not imply a divergent Loitsyansky integral, because, as explained in [5],

$$I_L = \lim_{V \rightarrow \infty} \langle |\mathbf{L}_V|^2 \rangle / V \quad (\text{B10})$$

is only formally valid when  $\mathbf{P}_V = 0$  – from Eq. (B1), we see that this is not the case. In [5], it is argued that this result means that any link between the Loitsyansky integral and angular momentum conservation is lost for turbulence with  $\mathbf{P}_V \neq 0$ . However, we point out that for eddies whose translational velocity is much smaller than the velocity associated with their rotation,  $U_t \ll U_r$ , and as long as  $R/L \ll (U_r/U_t)^2$ , Eq. (B9) is valid. This suggests that we might identify the limit  $V \rightarrow \infty$  as requiring  $L \ll V \ll (U_r/U_t)^2 L$ , and interpret the conservation of the Loitsyansky integral as the conservation of angular momentum associated with the eddies within such a volume.

In summary, while the scalings of  $\langle |\mathbf{P}_V|^2 \rangle$  and  $\langle |\mathbf{L}_V|^2 \rangle$  with  $R$  are modified from the naïve  $R^3$ , a correct application of the random-walk argument, taking into account incompressibility, and the greater contribution of more distant structures to  $\langle |\mathbf{L}_V|^2 \rangle$ , does result in the correct scalings. We therefore do not consider there to be an essential problem with the application of the random-walk argument in our treatment of the Saffman helicity invariant in Section III B, or in our discussion of general invariants in Section IV B.

### Appendix C: Numerical setup and simulation details

In this work, we have presented numerical simulations conducted with the spectral MHD code Snoopy [28]. The code solves the equations of incompressible MHD with hyper-viscosity and hyper-resistivity both of order  $n$ . In all our runs,  $\text{Pm} \equiv \nu_n / \eta_n = 1$ . The code employs a pseudospectral algorithm in a periodic box of size  $2\pi$ , with a 2/3 dealiasing rule. Units of time are chosen so that the initial magnetic energy is  $E_M = 1/2$  (i.e., the unit of time is the initial Alfvén crossing time of the box).

We initialise the simulations with a magnetic field whose Fourier representation is

$$B_i(\mathbf{k}) = \left[ i\epsilon_{ijk} \frac{k_k}{k} + s P_{ij}(\mathbf{k}) \right] F(k) G_j(\mathbf{k}), \quad (\text{C1})$$

where  $P_{ij}(\mathbf{k}) = \delta_{ij} - k_i k_j / k^2$  is the projection operator perpendicular to  $\mathbf{k}$ ,  $G_i(\mathbf{k})$  is the Fourier transform of a two- or three-dimensional Gaussian random field with zero correlation length. The parameter  $s$  controls the helicity –  $s = 1$  for a helical field,  $s = 0$  for a non-helical field – and is related to the fractional helicity,  $\sigma$ , discussed in Section IV A by  $\sigma = 2s/(1+s^2)$  [29]. The function  $F(k)$  sets the initial spectrum of the field:

$$F(k) = A \begin{cases} k^{(a-D+1)/2}, & k < k_c, \\ k^{(a-D+1)/2} \exp(1 - k^2/k_c^2), & k > k_c, \end{cases} \quad (\text{C2})$$

where  $D = 2, 3$  is the number of spatial dimensions,  $a$  is the initial spectral exponent of the sub-inertial range (small  $k$ ), and  $k_c$  sets the initial peak of the magnetic-energy spectrum,  $k_p$ , via  $k_p = (7/4)^{1/2} k_c$ . In all runs,

we set  $a = 7$ , and  $k_c = 25 \implies k_p \simeq 33$ , so that the magnetic energy is initialised at scales  $\simeq 1/33$  of the box size.

Other authors have attributed special significance to the initial sub-inertial-range spectral slope,  $a$  [19, 30]. However, we point out that the slope attained by the system after a few dynamical times is a kinematic consequence of the statistics of eddies at the energy-containing scale (see [5] for a theoretical explanation, [15] for a numerical study confirming this conclusion), and is, therefore, not a free parameter. Indeed, we found in exploratory runs that the transient period before the system entered a period of power-law decay was shorter when the large-scale slope was allowed to establish itself organically, from an initial steep slope (which happens in a few dynamical timescales), than when we artificially imposed the expected values, which are  $a = 3$  in two dimensions, and  $a = 4$  in three dimensions [5] (see Figs. 2 and 7). Presumably, this is because even if the spectral exponent is the right one, the structure of the synthetic field, Eq. (C1) is not, so it is better not to prejudice the system and let it decide for itself what structures to create at large scales ( $k < k_p$ ).

We measure the decay exponents  $p_M$  and  $p_K$  by plotting  $|E_i^{1+1/p_i} dE_i/dt|$  against time, selecting the parameter  $p_i$  ( $i = M, K$ ) so as to obtain a flat curve. As noted in [9], plots of this type give an unbiased estimate of the decay laws, as compared to more conventional logarithmic plots of  $E$  against  $t$ . The reason for this is that, because the power-law behaviour is only established after a short time  $t_0$  following the initialization of the simulation, a plot of  $E \sim (t - t_0)^{-p}$  against  $t$  has a bias towards large energies, which decreases over time, giving the false impression of a steeper power law. Furthermore, a logarithmic  $t$ -axis exaggerates the importance of the initial times, during which the system has, in fact, not established a steady-state decay. In a similar way, we establish the value of  $\alpha$  in Eq. (10) by plotting  $E_M^{\alpha/2} L$  against time and selecting the value of  $\alpha$  to give a flat curve. The power laws and values of  $\alpha$  thus obtained are given for all our runs in Table I, together with the resolution and initial Lundquist number for each run. For reference, the plots from which these results are obtained are shown in Figs. 12, 13 and 14. Also plotted there are the curves obtained using the values of  $p_M$ ,  $p_K$ , and  $\alpha$  at the extremes of the error bars in Figs. 1, 2(b), 6, 7(b) and 11, to give a sense of the precision with which these results hold.

Type	$n$	Resolution	$\eta_n = \nu_n$	$S_{n,0}^{1/n}$	$\alpha$	$p_M$	$p_K$
H.	2	$576^3$	$8.92 \times 10^{-4}$	14.59	0.93	1.07	1.20
H.	2	$576^3$	$6.08 \times 10^{-4}$	17.68	1.16	0.85	1.00
H.	2	$576^3$	$4.14 \times 10^{-4}$	21.42	1.37	0.76	0.92
H.	2	$576^3$	$2.82 \times 10^{-4}$	25.93	1.52	0.70	0.85
H.	2	$576^3$	$1.92 \times 10^{-4}$	31.44	1.64	0.69	0.83
H.	2	$576^3$	$1.31 \times 10^{-4}$	38.09	1.74	0.66	0.85
H.	4	$576^3$	$2.00 \times 10^{-5}$	4.30	0.30	1.80	1.15
H.	4	$576^3$	$9.28 \times 10^{-6}$	5.21	0.45	1.25	1.20
H.	4	$576^3$	$6.32 \times 10^{-6}$	5.74	0.58	1.00	1.15
H.	4	$576^3$	$4.31 \times 10^{-6}$	6.32	0.90	0.75	0.97
H.	4	$576^3$	$2.94 \times 10^{-6}$	6.95	1.40	0.59	0.76
H.	4	$576^3$	$2.00 \times 10^{-6}$	7.65	1.60	0.56	0.95
H.	4	$576^3$	$2.00 \times 10^{-7}$	13.61	1.93	0.56	0.95
H.	4	$576^3$	$2.00 \times 10^{-8}$	24.20	1.99	0.56	0.91
H.	4	$1152^3$	$2.00 \times 10^{-9}$	43.03	2.00	0.56	0.90
H.	6	$576^3$	$4.48 \times 10^{-11}$	13.29	1.98	0.60	0.90
H.	6	$576^3$	$1.42 \times 10^{-12}$	23.64	2.00	0.60	1.00
NH.	2	$576^3$	$8.92 \times 10^{-4}$	14.59	0.46	2.10	1.95
NH.	2	$576^3$	$6.08 \times 10^{-4}$	17.68	0.49	1.90	1.90
NH.	2	$576^3$	$4.14 \times 10^{-4}$	21.42	0.53	1.75	1.75
NH.	2	$576^3$	$2.82 \times 10^{-4}$	25.93	0.56	1.59	1.59
NH.	2	$576^3$	$1.92 \times 10^{-4}$	31.44	0.60	1.50	1.40
NH.	2	$576^3$	$1.31 \times 10^{-4}$	38.09	0.65	1.40	1.32
NH.	4	$576^3$	$5.0 \times 10^{-6}$	6.09	0.48	1.25	1.30
NH.	4	$576^3$	$2.0 \times 10^{-6}$	7.65	0.46	1.30	1.30
NH.	4	$576^3$	$1.0 \times 10^{-6}$	9.10	0.60	1.05	1.20
NH.	4	$576^3$	$5.0 \times 10^{-7}$	10.82	0.72	1.00	1.05
NH.	4	$576^3$	$2.0 \times 10^{-7}$	13.61	0.75	1.03	1.08
NH.	4	$576^3$	$2.0 \times 10^{-8}$	24.20	0.78	1.03	1.13
NH.	4	$1152^3$	$2.0 \times 10^{-9}$	43.03	0.80	1.04	1.12
NH.	6	$576^3$	$4.48 \times 10^{-11}$	13.29	0.80	1.00	1.05
NH.	6	$576^3$	$1.42 \times 10^{-12}$	23.64	0.80	1.03	1.20
2D	2	$1152^2$	$8.92 \times 10^{-4}$	14.59	0.55	1.50	1.40
2D	2	$1152^2$	$2.82 \times 10^{-4}$	25.93	0.80	1.15	1.10
2D	2	$2304^2$	$8.92 \times 10^{-5}$	46.15	0.98	1.00	1.25
2D	2	$2304^2$	$2.82 \times 10^{-5}$	82.01	1.00	0.95	0.95
2D	2	$4608^2$	$8.92 \times 10^{-6}$	145.94	0.97	0.91	1.00
2D	4	$1152^2$	$2.0 \times 10^{-7}$	13.61	0.90	0.95	0.95
2D	4	$1152^2$	$2.0 \times 10^{-8}$	24.20	1.00	0.90	0.90
2D	4	$2304^2$	$2.0 \times 10^{-9}$	43.03	1.00	0.80	0.90
2D	4	$2304^2$	$2.0 \times 10^{-10}$	76.52	0.95	0.77	1.00
2D	4	$4608^2$	$2.0 \times 10^{-11}$	136.08	0.95	0.78	1.00
2D	6	$1152^2$	$4.48 \times 10^{-11}$	13.29	0.98	0.90	1.00
2D	6	$1152^2$	$1.42 \times 10^{-12}$	23.64	1.02	0.85	1.10
2D	6	$2304^2$	$4.48 \times 10^{-14}$	42.04	1.00	0.85	1.00
2D	6	$2304^2$	$1.42 \times 10^{-15}$	74.76	1.00	0.76	1.00
2D	6	$4608^2$	$4.48 \times 10^{-17}$	132.95	0.97	0.71	1.00

TABLE I. Details of all simulations, together with the measured decay exponents and the values of  $\alpha$  such that  $B^\alpha L \sim \text{const.}$

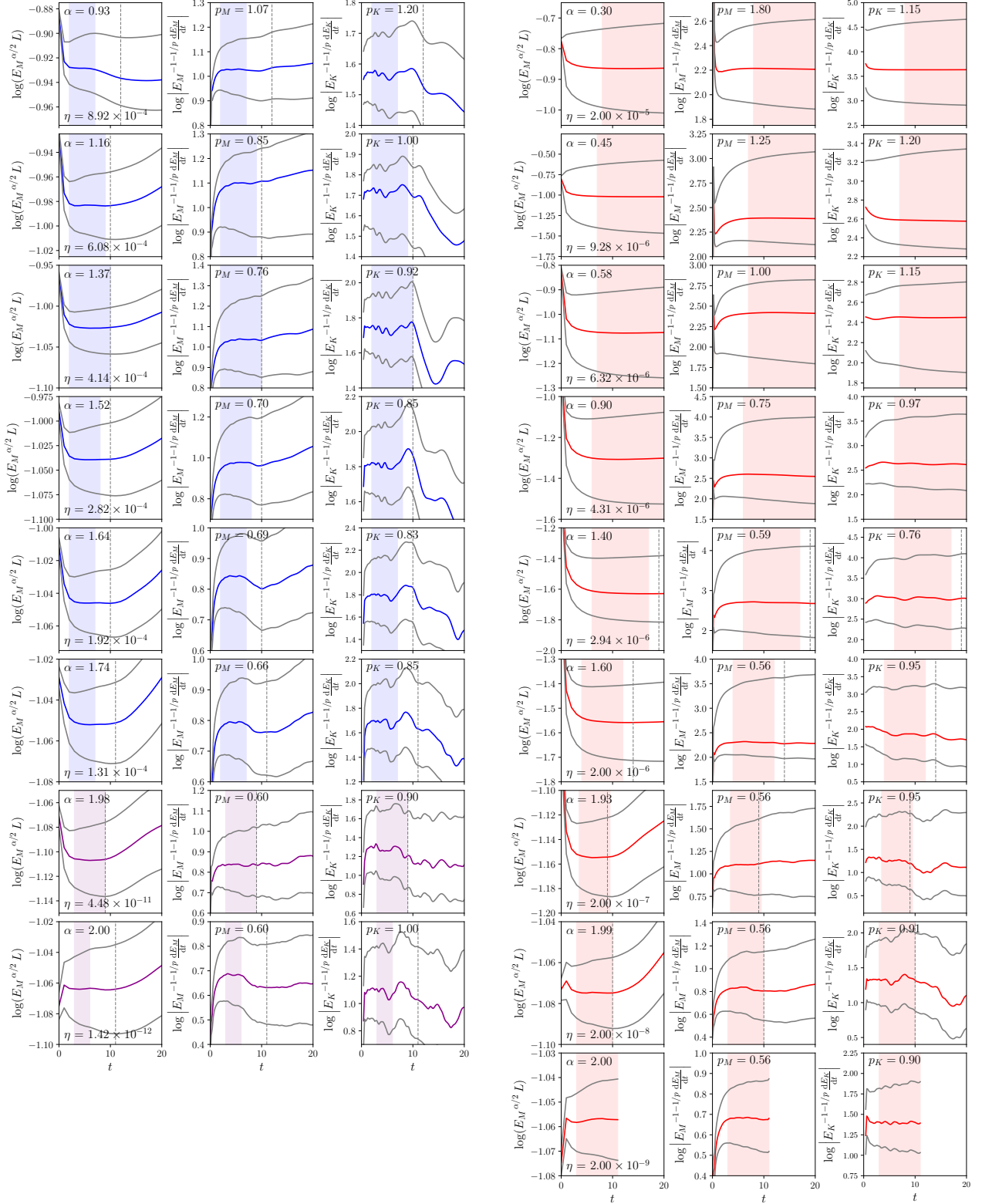


FIG. 12. Plots used to obtain the parameters  $\alpha$  (left),  $p_M$  (centre) and  $p_K$  (right), for each helical simulation. Simulations with  $n = 2$ ,  $n = 4$ , and  $n = 6$  hyper-dissipation are plotted in blue, red and magenta, respectively. In each case, a horizontal line indicates agreement with the stated value. The shaded region indicates the times at which the decay laws appear to be valid. Grey lines correspond to the values of  $\alpha$ ,  $p_M$ , and  $p_K$  at the extremes of the error bars shown in Figs. 6 and 7. Dashed lines show the time at which  $L = 2\pi/5$ , i.e., when magnetic structures have scale 1/5 of the box size, which we find to be roughly the time at which finite-box-size effects begin to affect the decay laws.

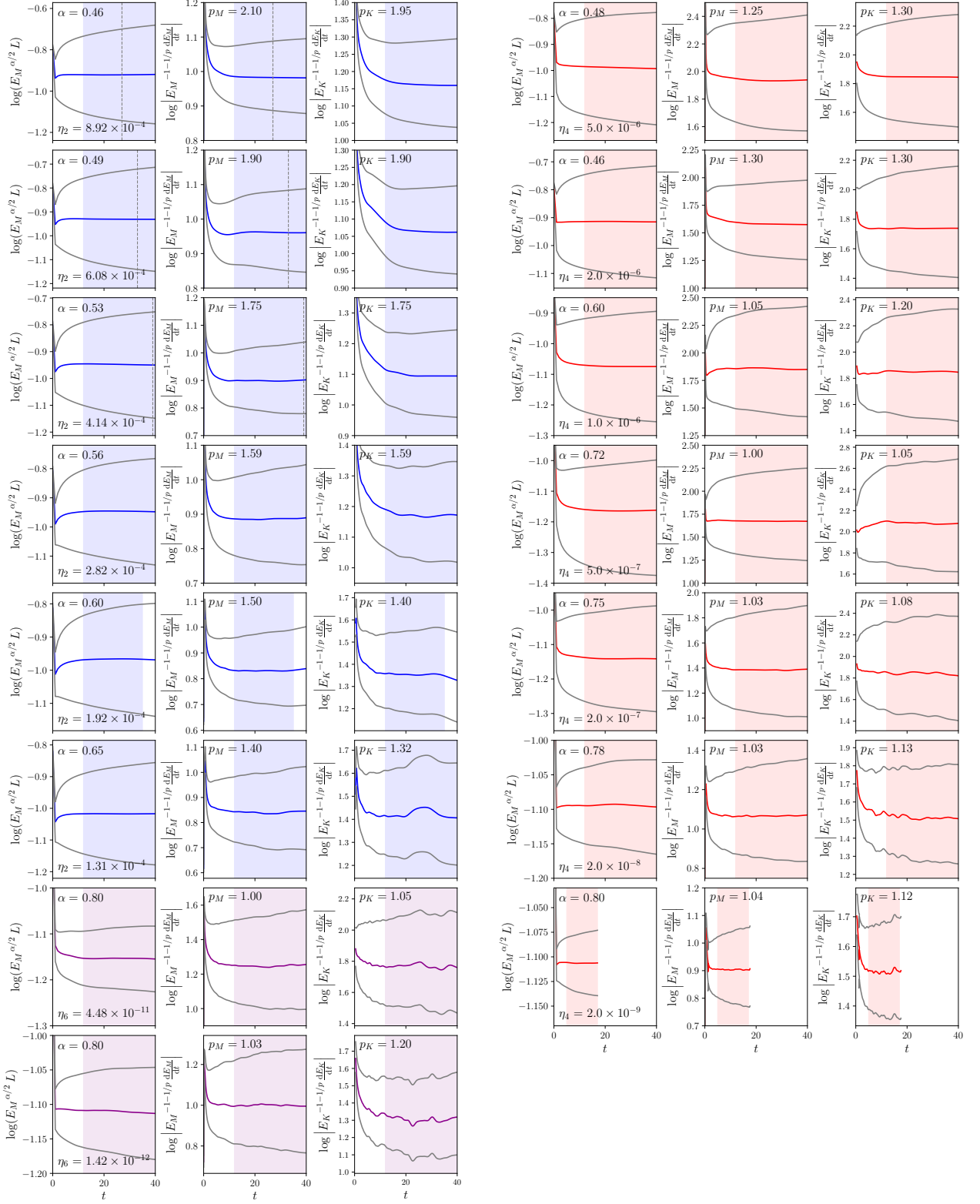


FIG. 13. Same as Fig. 12, but for non-helical simulations.

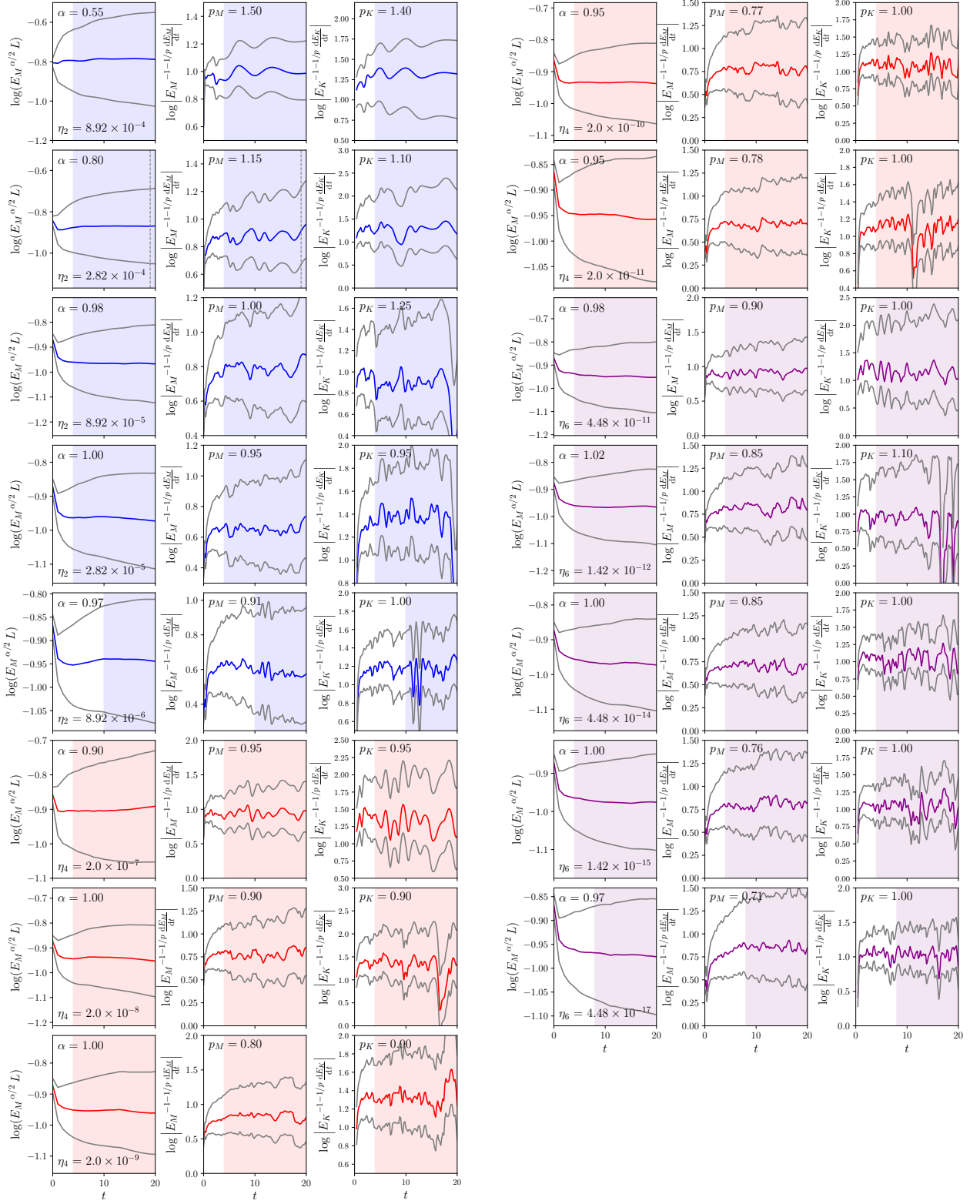


FIG. 14. Same as Fig. 12, but for two-dimensional simulations.

- 
- [1] R. Banerjee and K. Jedamzik, Evolution of cosmic magnetic fields: From the very early universe, to recombination, to the present, *Phys. Rev. D* **70**, 123003 (2004).
- [2] C. H. K. Chen, A. Mallet, T. A. Yousef, A. A. Schekochihin, and T. S. Horbury, Anisotropy of Alfvénic turbulence in the solar wind and numerical simulations, *Mon. Not. R. Astron. Soc.* **415**, 3219 (2011).
- [3] A. N. Kolmogorov, Dissipation of energy in locally isotropic turbulence, *Dokl. Acad. Nauk SSSR* **32**, 16 (1941).
- [4] L. D. Landau and E. M. Lifshitz, *Fluid mechanics* (Pergamon Press, 1959).
- [5] P. A. Davidson, *Turbulence in rotating, stratified and electrically conducting fluids* (Cambridge University Press, 2013).
- [6] T. Ishida, P. A. Davidson, and Y. Kaneda, On the decay of isotropic turbulence, *J. Fluid Mech.* **564**, 455 (2006).
- [7] T. Hatori, Kolmogorov-style argument for the decaying homogeneous MHD turbulence, *J. Phys. Soc. Jpn* **53**, 2539 (1984).
- [8] D. Biskamp and H. Welter, Dynamics of decaying two-dimensional magnetohydrodynamic turbulence, *Phys. Fluids B* **1**, 1964 (1989).
- [9] D. Biskamp and W.-C. Müller, Decay laws for three-dimensional magnetohydrodynamic turbulence, *Phys. Rev. Lett.* **83**, 2195 (1999).
- [10] D. T. Son, Magnetohydrodynamics of the early universe and the evolution of primordial magnetic fields, *Phys. Rev. D* **59**, 063008 (1999).
- [11] W.-C. Müller and D. Biskamp, Scaling properties of three-dimensional magnetohydrodynamic turbulence, *Phys. Rev. Lett.* **84**, 475 (2000).
- [12] M. Christensson, M. Hindmarsh, and A. Brandenburg, Inverse cascade in decaying three-dimensional magnetohydrodynamic turbulence, *Phys. Rev. E* **64**, 056405 (2001).
- [13] P. Frick and R. Stepanov, Long-term free decay of MHD turbulence, *Europhys. Lett.* **92**, 34007 (2010).
- [14] A. Berera and M. Linkmann, Magnetic helicity and the evolution of decaying magnetohydrodynamic turbulence, *Phys. Rev. E* **90**, 041003 (2014).
- [15] A. Brandenburg and T. Kahniashvili, Classes of hydrodynamic and magnetohydrodynamic turbulent decay, *Phys. Rev. Lett.* **118**, 055102 (2017).
- [16] D. Biskamp and U. Bremer, Dynamics and statistics of inverse cascade processes in 2D magnetohydrodynamic turbulence, *Phys. Rev. Lett.* **72**, 3819 (1994).
- [17] W.-C. Müller, S. K. Malapaka, and A. Busse, Inverse cascade of magnetic helicity in magnetohydrodynamic turbulence, *Phys. Rev. E* **85**, 015302 (2012).
- [18] J. Zrake, Inverse cascade of nonhelical magnetic turbulence in a relativistic fluid, *Astrophys. J. Lett.* **794**, L26 (2014).
- [19] A. Brandenburg, T. Kahniashvili, and A. e. G. Tevzadze, Nonhelical inverse transfer of a decaying turbulent magnetic field, *Phys. Rev. Lett.* **114**, 075001 (2015).
- [20] J. Reppin and R. Banerjee, Nonhelical turbulence and the inverse transfer of energy: a parameter study, *Phys. Rev. E* **96**, 053105 (2017).
- [21] K. Park, On the inverse transfer of (non-)helical magnetic energy in a decaying magnetohydrodynamic turbulence, *Mon. Not. R. Astron. Soc.* **472**, 1628 (2017).
- [22] P. Bhat, M. Zhou, and N. F. Loureiro, Inverse energy transfer in decaying, three dimensional, nonhelical magnetic turbulence due to magnetic reconnection, arXiv , 2007.07325 (2020).
- [23] M. Zhou, P. Bhat, N. F. Loureiro, and D. A. Uzdensky, Magnetic island merger as a mechanism for inverse magnetic energy transfer, *Phys. Rev. Res.* **1**, 012004 (2019).
- [24] D. A. Uzdensky, N. F. Loureiro, and A. A. Schekochihin, Fast magnetic reconnection in the plasmoid-dominated regime, *Phys. Rev. Lett.* **105**, 235002 (2010).
- [25] A. Lazarian, G. L. Eyink, A. Jafari, G. Kowal, H. Li, S. Xu, and E. T. Vishniac, 3D turbulent reconnection: theory, tests, and astrophysical implications, *Phys. Plasmas* **27**, 012305 (2020).
- [26] P. A. Sweet, The neutral point theory of solar flares, in *Electromagnetic Phenomena in Cosmical Physics*, Vol. 6, edited by B. Lehnert (1958) p. 123.
- [27] E. N. Parker, Sweet’s mechanism for merging magnetic fields in conducting fluids, *J. Geophys. Res.* **62**, 509 (1957).
- [28] G. Lesur, Snoopy: general purpose spectral solver, Astrophysics Source Code Library (ascl:1505.022) (2015).
- [29] A. Brandenburg, T. Kahniashvili, S. Mandal, A. R. Pol, A. G. Tevzadze, and T. Vachaspati, Dynamo effect in decaying helical turbulence, *Phys. Rev. Fluids* **4**, 024608 (2019).
- [30] P. Olesen, Inverse cascades and primordial magnetic fields, *Phys. Lett. B* **398**, 321 (1997).
- [31] L. Campanelli, Scaling laws in magnetohydrodynamic turbulence, *Phys. Rev. D* **70**, 083009 (2004).
- [32] P. G. Saffman, The large-scale structure of homogeneous turbulence, *J. Fluid Mech.* **27**, 581 (1967).
- [33] P. A. Davidson, N. Okamoto, and Y. Kaneda, On freely decaying, anisotropic, axisymmetric Saffman turbulence, *J. Fluid Mech.* **706**, 150 (2012).
- [34] M. Zhou, N. F. Loureiro, and D. A. Uzdensky, Multi-scale dynamics of magnetic flux tubes and inverse magnetic energy transfer, *J. Plasma Phys.* **86**, 535860401 (2020).
- [35] A. Ruzmaikin and P. Akhmetiev, Topological invariants of magnetic fields, and the effect of reconnections, *Phys. Plasmas* **1**, 331 (1994).
- [36] M. A. Berger, Rigorous new limits on magnetic helicity dissipation in the solar corona, *Geophys. Astrophys. Fluid Dyn.* **30**, 79 (1984).
- [37] J. B. Taylor, Relaxation of toroidal plasma and generation of reverse magnetic fields, *Phys. Rev. Lett.* **33**, 1139 (1974).
- [38] H. K. Moffatt, Magnetostatic equilibria and analogous Euler flows of arbitrarily complex topology. I - Fundamentals, *J. Fluid Mech.* **159**, 359 (1985).
- [39] H. R. Strauss, Nonlinear, three-dimensional magnetohydrodynamics of noncircular tokamaks, *Phys. Fluids* **19**, 134 (1976).
- [40] B. B. Kadomtsev and O. P. Pogutse, Nonlinear helical perturbations of a plasma in the tokamak, *Soviet Phys. JETP* **38**, 283 (1974).
- [41] J. C. Perez and S. Boldyrev, Role of cross-helicity in magnetohydrodynamic turbulence, *Phys. Rev. Lett.* **102**, 025003 (2009).
- [42] M. Wan, S. Oughton, S. Servidio, and W. H. Matthaeus,

- von Kármán self-preservation hypothesis for magnetohydrodynamic turbulence and its consequences for universality, *J. Fluid Mech.* **697**, 296 (2012).
- [43] E. Lee, M. E. Brachet, A. Pouquet, P. D. Mininni, and D. Rosenberg, Lack of universality in decaying magnetohydrodynamic turbulence, *Phys. Rev. E* **81**, 016318 (2010).
- [44] P. Goldreich and S. Sridhar, Toward a theory of interstellar turbulence. II. Strong Alfvénic turbulence, *Astrophys. J.* **438**, 763 (1995).
- [45] S. V. Nazarenko and A. A. Schekochihin, Critical balance in magnetohydrodynamic, rotating and stratified turbulence: towards a universal scaling conjecture, *J. Fluid Mech.* **677**, 134 (2011).
- [46] A. Mallet, A. A. Schekochihin, and B. D. G. Chandran, Refined critical balance in strong Alfvénic turbulence., *Mon. Not. R. Astron. Soc.* **449**, L77 (2015).
- [47] J. Maron and P. Goldreich, Simulations of incompressible magnetohydrodynamic turbulence, *Astrophys. J.* **554**, 1175 (2001).
- [48] S. Oughton, E. R. Priest, and W. H. Matthaeus, The influence of a mean magnetic field on three-dimensional magnetohydrodynamic turbulence, *J. Fluid Mech.* **280**, 95 (1994).
- [49] J. Cho, A. Lazarian, and E. T. Vishniac, Simulations of magnetohydrodynamic turbulence in a strongly magnetized medium, *Astrophys. J.* **564**, 291 (2002).
- [50] F. Rincon, Dynamo theories, *J. Plasma Phys.* **85**, 205850401 (2019).
- [51] A. A. Schekochihin, MHD turbulence: a biased review, arXiv , 2010.00699 (2020).
- [52] A. A. Schekochihin, Y. Kawazura, and M. A. Barnes, Constraints on ion versus electron heating by plasma turbulence at low beta, *J. Plasma Phys.* **85**, 905850303 (2019).
- [53] R. Meyrand, J. Squire, A. A. Schekochihin, and W. Dorland, Violation of the zeroth law of turbulence in space plasmas, arXiv , 2009.02828 (2020).
- [54] L. M. Milanese, N. F. Loureiro, M. Daschner, and S. Boldyrev, Dynamic phase alignment in inertial Alfvén turbulence, arXiv , 2010.00415 (2020).